Observer based optical manipulation of biological cells with robotic tweezers

Li, Xiang; Yan, Xiao; Sun, Dong; Cheah, Chien Chern

2013

Cheah, C. C., Li, X. Yan, X., & Sun, D. (2013). Observer based optical manipulation of biological cells with robotic tweezers. IEEE transactions on robotics, PP(99), 1-13.

https://hdl.handle.net/10356/101577

Observer Based Optical Manipulation of Biological Cells with Robotic Tweezers

Chien Chern Cheah, *Senior Member, IEEE,* Xiang Li, *Member, IEEE,* Xiao Yan, *Member, IEEE,* and Dong Sun, *Senior Member, IEEE,*

***Abstract*—While several automatic manipulation techniques have been developed for optical tweezers system recently, the measurement of the velocity of cell is required and the interaction between the cell and the manipulator of laser source is usually ignored in these formulations. Although the position of cell can be measured by using a camera, the velocity of cell is not measurable and usually estimated by differentiating the position of cell, which amplifies noises and may induce chattering of the system. In addition, it is also assumed in existing methods that the image Jacobian matrix from Cartesian space to image space of the camera is exactly known. In the presence of estimation errors or variations of depth information between the camera and the cell, it is not sure whether the stability of the system could still be ensured. In this paper, vision based observer techniques are proposed for optical manipulation to estimate the velocity of cell. Using the proposed observer techniques, tracking control strategies are developed to manipulate biological cells with different Reynolds' number, which do not require camera calibration and measurement of the velocity of cell. The control methods are based on the dynamic formulation where the laser source is controlled by closed-loop robotic manipulation technique. The stability is analysed using Lyapunov-like analysis. Simulation and experimental results are presented to illustrate the performance of the proposed cell manipulation methods.**

***Index Terms*—Cell manipulation, optical tweezers, vision based control, observer based control.**

I. INTRODUCTION

ROBOTIC technologies have been demonstrated as key drivers in manufacturing automation. The integration of robotic and biomedical technologies at miro and nano scales has led to the emergence of a variety of robotic cell manipulation systems with ultrahigh precision, such as micro insertion system [1], micro-gripper [2], [3], injection system [4], [5], and micropipette [6], [7].

Among many types of manipulation systems, optical tweezers [8] have become indispensable tools in biological and nanotechnological fields, because of the capability of manipulating microscopic objects precisely without any physical contact. Using a highly focused laser beam, optical tweezers allow scientists to carry out studies for a diversity of objects including atoms, molecules, bacteria, viruses and biological cells [9]. Over the past few years, the design, development, and utilization of optical tweezers have increased significantly, and various automatic optical manipulation systems and control techniques have been developed [10]–[20]. In [10], an automatic micromanipulation system with a configuration of dual-beam optical trap was developed for cell separation. An automated optical trapping system was proposed by using computer vision techniques and multiple-force optical clamps in [11]. In [12], a 3-D steering system was developed for optical tweezers, with a combination of deformable mirror and acousto-optic deflector. Based on a first-order dynamic model of the cell, a comparison was perform for several classic control methods to evaluate their performance for optical manipulation in [13]. In [14], a proportional-gain feedback controller was implemented on optical tweezers. In [15], a weighted-recursive-least-square algorithm was proposed for real-time calibration and estimation of system parameters. A minimum variance control method was proposed to minimize the Brownian motion of an optically trapped probe in [16] and an adaptive minimum variance control was also demonstrated experimentally. In [17], an adaptive disturbance observer was developed for on-line estimation of probe-sample interaction force in an optical trap. To transport a single microscopic particle to a desired point, a simple regulation controller was proposed for optical tweezers in [18]. A PI feedback controller and a synchronization control technology were proposed for cell transportation using optical tweezers in [19]. A region reaching control method was developed for flocking multiple micro particles in [20].

In aforementioned robotic manipulation techniques using optical tweezers [13]–[20], the control input is usually treated as the position of the laser beam, and open-loop controllers are designed to move the laser source by ignoring the interaction between the manipulator of the laser source and the cell. The dynamic interaction between the robotic manipulator and the cell was first considered in [21], [22]. A dynamic formulation that takes into account the combined effects of manipulator and cell is proposed for optical tweezers systems, so that the position of the laser source can be controlled by closed-loop techniques. However, the overall or full dynamic equation that include the dynamics of both the cell and the manipulator, is a third or fourth-order system, and higher-order derivatives and the velocity of cell are required for the control input of the robotic manipulator. Some techniques are proposed to eliminate the requirement of the acceleration information and its derivatives [22], [23], but the measurement of the velocity of cell is still required for the control laws.

C. C. Cheah, and X. Li are with the School of Electrical and Electronic Engineering, Nanyang Technological University, Singapore, and X. Yan, and D. Sun are with the Department of Mechanical and Biomedical Engineering, City University of Hong Kong, Hong Kong S.A.R, P.R.China. The work of the first and second authors was supported by the Agency For Science, Technology And Research of Singapore (A*STAR), (Reference No. 1121202014), and the work of the third and last authors was supported in part by the Research Grants Council of the Hong Kong Special Administrative Region, China (Reference No. CityU 119612).

In these control schemes for cell manipulation systems [5], [6], [19]–[23], the velocity feedback of the cell is required for the control tasks. However, in actual implementations of the controllers, the velocity of cell cannot be measured directly from the camera and is usually estimated by differentiating the position of cell. The differentiation amplifies noise at high frequencies and may cause chattering which is not desirable for cell manipulation. Even if the velocity feedback of the cell is not used in open-loop control of laser source, it is still needed in closed-loop control of the manipulator of laser source. In addition, it is assumed that the relationship between Cartesian space and image space of the camera is known exactly. In the presence of estimation errors or variations of depth information between the camera and the cell, the sensory transformation from the task error in image space to the control input in Cartesian space is uncertain and hence it is not sure whether the stability of the system could still be ensured. While a great quantity of work has been reported in the literature of robot visual servoing [24], [25] and velocity observer [26]–[29], the uncalibrated vision based optical manipulation problem of cells or nanoparticles without measurement of the velocity has not been solved.

In this paper, observer based control schemes are proposed for optical manipulation of biological cells without measurement of the velocity of cell. The proposed methods are based on the dynamic formulation where the position of laser beam is controlled by vision based closed-loop robotic manipulation techniques. The relationship from the Cartesian space to the image space of microscope is described by an image Jacobian matrix, which directly transforms the image-space sensory feedback error into the control input of manipulator. Vision based observer techniques are developed to estimate the velocity and the position of the cell. Using the proposed observer techniques, the optical tweezers system is able to manipulate the cell to follow a time-varying trajectory without camera calibration and measurement of the velocity of cell. Various control methods are proposed for manipulation of biological cells with different Reynolds' number, which is dependent on the dimension of cell and manipulation environment. The stability of the closed-loop system is analysed by using Lyapunov-like methods. Both simulation and experimental results are presented to illustrate the performance of the proposed control schemes.

II. Optical Tweezers System

A. Principle of Optical Trap

The basic principle of optical trap is based on the transfer of momentum from photons to the biological cell, when a focused beam of light travels through the cell that is immersed in a medium. The refraction of the photons at the boundary between the cell and the medium, results in a stable trap of the object [8]. The trapped cell mainly experiences the trapping force from the optical trap and the viscous drag force from the environment. The dynamic model of the cell can be described as follows [20]:

$$\boldsymbol{M}\ddot{\boldsymbol{x}} = \boldsymbol{F}_{trap} - \boldsymbol{F}_{drag}, \tag{1}$$

where $\boldsymbol{M} \in \Re^{2\times 2}$ represents the mass matrix of the cell which is diagonal and positive definite, $\ddot{\boldsymbol{x}}$ is the acceleration of the trapped cell, $\boldsymbol{F}_{trap}$ denotes the trapping force, and $\boldsymbol{F}_{drag}$ denotes the drag force.

The drag force $\boldsymbol{F}_{drag}$ is proportional to the velocity of the cell. i.e. $\boldsymbol{F}_{drag} = \boldsymbol{B}\dot{\boldsymbol{x}}$, where $\boldsymbol{B} \in \Re^{2\times 2}$ represents the damping matrix which is also diagonal and positive definite, and $\dot{\boldsymbol{x}}$ is the velocity of the cell. The trapping force $\boldsymbol{F}_{trap}$ can be represented as the product of a trapping stiffness and the offset between the cell and the center of laser beam as: $\boldsymbol{F}_{trap} = -\boldsymbol{K}(\boldsymbol{x}-\boldsymbol{p})$, where $\boldsymbol{K}$ denotes the trap stiffness matrix which is positive definite, $\boldsymbol{x} = [x_1, x_2]^T \in \Re^2$ is the position of the cell, and $\boldsymbol{p} = [p_1, p_2]^T \in \Re^2$ is the position of the laser beam. Both $\boldsymbol{x}$ and $\boldsymbol{p}$ are usually specified in the image space of the microscope $\sum_C$. When the cell is very near the laser beam, $\boldsymbol{K}$ is constant, and the trapping force $\boldsymbol{F}_{trap}$ is proportional to the offset $\boldsymbol{x}-\boldsymbol{p}$, and hence the cell can be trapped by the laser beam, as illustrated in Fig. 1.

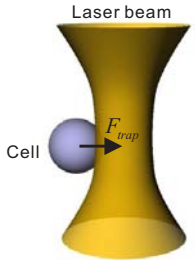

Fig. 1. The cell can be trapped by the laser beam when it is very near the laser beam.

In this paper, we assume that the cell has been trapped by the laser beam and the stiffness of the trapping force is constant [18]–[20]. Therefore, the dynamic equation of the trapped cell (1) can be written as:

$$\boldsymbol{M}\ddot{\boldsymbol{x}} + \boldsymbol{B}\dot{\boldsymbol{x}} + \boldsymbol{K}(\boldsymbol{x}-\boldsymbol{p}) = \boldsymbol{0}. \tag{2}$$

Various microscopic objects can be trapped by the laser beam. As the dimension of the object decreases, the Reynolds' number [30]–[33] decreases. When a biological cell is manipulated by the laser beam with a low Reynolds' number, viscous drag dominates inertia due to the scaling effect. That is, the mass of the cell can be ignored, and the model of the trapped cell (2) is simplified as [13], [18], [19]:

$$\boldsymbol{B}\dot{\boldsymbol{x}} + \boldsymbol{K}(\boldsymbol{x}-\boldsymbol{p}) = \boldsymbol{0}. \tag{3}$$

B. Manipulation with Optical Trap

Optical tweezers are the scientific instruments based on the optical trap, which can manipulate microscopic objects without physical contact. A typical optical manipulation system is shown in Fig. 2. The main features consist of a large numerical aperture oil-immersion objective, a standard phase contrast microscope illumination, and a CCD camera.

In this paper, the position of the laser beam is specified with respect to the stage of optical tweezers, and it is controlled by closed-loop robotic manipulation techniques. The dynamics of the manipulator of the laser source is described as [22]:

$$\boldsymbol{M}_q\ddot{\boldsymbol{q}} + \boldsymbol{B}_q\dot{\boldsymbol{q}} = \boldsymbol{u}, \tag{4}$$

where $\boldsymbol{q} = [q_1, q_2]^T$ is the position of the laser beam with respect to the stage in Cartesian space. The matrix $\boldsymbol{M}_q \in \Re^{2\times 2}$ represents the mass matrix which is diagonal and positive definite, $\boldsymbol{B}_q \in \Re^{2\times 2}$ represents the damping matrix which is also diagonal and positive definite, and $\boldsymbol{u} \in \Re^2$ is the control input for the manipulator.

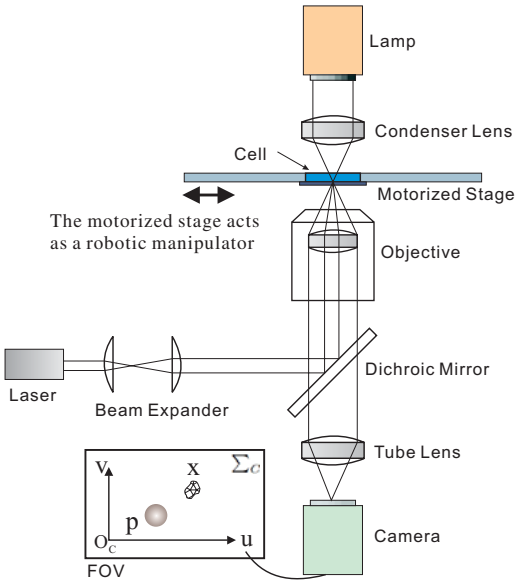

Fig. 2. A typical optical tweezers system.The offset between the cell and the laser can be varied by the motorized stage which acts as a robotic manipulator.

C. Camera Model

In optical tweezers system, the relationship between the Cartesian space of the motorized stage and the image space of the microscope is defined by the pinhole camera model [24], [34], which is illustrated in Fig. 3. Based on the pinhole camera model, the velocity of image feature is related to the velocity of feature point in Cartesian space by using the image Jacobian matrix [35], [36] as:

$$\dot{\boldsymbol{p}} = \boldsymbol{J}_I(\boldsymbol{q})\dot{\boldsymbol{q}}, \tag{5}$$

where $\boldsymbol{J}_I(\boldsymbol{q})$ is the image Jacobian matrix, $\dot{\boldsymbol{p}}$ is the image-space velocity of laser beam, and $\dot{\boldsymbol{q}}$ is the velocity of laser beam in Cartesian space. If the laser beam evolves in the 2-D plane of the stage while the camera is perpendicular to the evolving plane of the laser beam, the image Jacobian matrix is constant. If the cell is submerged in a 3D space, the depth information is not constant. In the case that other manipulation systems such as a beam steering system [37] is employed as a manipulator to control the position of laser beam, the image Jacobian matrix is also nonlinear.

III. Observer Based Optical Manipulation

In optical manipulation of biological cells, the information about the position and velocity is required for tracking control. Both the position of cell $\boldsymbol{x}$ and the position of laser source $\boldsymbol{p}$ in image space can be measured by using the camera. However, the velocity of cell cannot be measured by the camera directly.

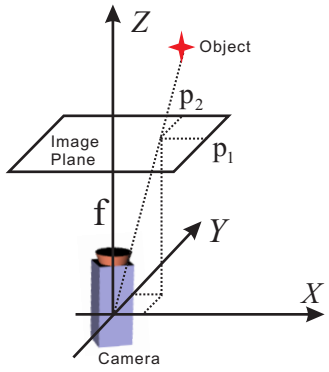

Fig. 3. The projection for a pinhole camera model, where f is the focal length of the camera, and $\boldsymbol{p} = [p_1, p_2]^T$ represents the position of the laser beam in image space.

In this section, vision based observer techniques are employed to eliminate the requirement of using the velocity of cell for optical manipulation. We first consider the cell manipulation with a low Reynolds' number, and then extend the results to the case of a high Reynolds' number.

The development of the vision-based control techniques for optical tweezers is based on a backstepping approach [38]. First, based on the cell dynamics in equations (2) or (3), a desired position input of laser beam $\boldsymbol{p}_d$ is developed in image space to ensure the convergence of tracking errors of cell. Second, based on the manipulator dynamics in equation (4), a control input $\boldsymbol{u}$ for the robotic manipulator of the laser source is developed to ensure that the actual position of the laser beam in image space $\boldsymbol{p}$ tracks the desired position input $\boldsymbol{p}_d$.

A. Optical Manipulation of Cell with Low Reynolds' Number

When the cell with a low Reynolds' number is manipulated by the optical tweezers, the dynamic model of the cell is described by equation (3). Suppose that the desired position input for the laser beam is denoted as $\boldsymbol{p}_d$, then equation (3) can be written as:

$$\boldsymbol{B}\dot{\boldsymbol{x}} + \boldsymbol{K}\boldsymbol{x} = \boldsymbol{K}\Delta\boldsymbol{p} + \boldsymbol{K}\boldsymbol{p}_d. \tag{6}$$

where $\Delta\boldsymbol{p} = \boldsymbol{p} - \boldsymbol{p}_d$ represents an input perturbation to the cell dynamics. The system in equation (6) can be viewed as being controlled by the input $\boldsymbol{K}\boldsymbol{p}_d$ with the perturbation $\boldsymbol{K}\Delta\boldsymbol{p}$.

Based on the simplified dynamic model of the trapped cell, a vision based observer is developed to estimate the velocity of the cell as:

$$\dot{\hat{\boldsymbol{x}}} = \boldsymbol{B}^{-1}[-\boldsymbol{K}(\boldsymbol{x} - \boldsymbol{p}) + \boldsymbol{K}_x\boldsymbol{e}_x], \tag{7}$$

where $\hat{\boldsymbol{x}}$ is the estimated position of the trapped cell, $\dot{\hat{\boldsymbol{x}}}$ is the estimated velocity, $\boldsymbol{e}_x = \boldsymbol{x} - \hat{\boldsymbol{x}}$ is the observation error, and $\boldsymbol{K}_x$ is a diagonal and positive definite matrix. The estimated position $\hat{\boldsymbol{x}}$ is obtained by integrating the estimated velocity $\dot{\hat{\boldsymbol{x}}}$. Using $\hat{\boldsymbol{x}}$, the desired position input for the laser beam is proposed as:

$$\boldsymbol{p}_d = \hat{\boldsymbol{x}} - \boldsymbol{K}^{-1}\boldsymbol{K}_p\Delta\hat{\boldsymbol{x}} + \boldsymbol{K}^{-1}\boldsymbol{B}\dot{\boldsymbol{x}}_d, \tag{8}$$

where $\boldsymbol{K}_p$ is the proportional control gain matrix which is diagonal and positive definite, $\Delta\hat{\boldsymbol{x}} = \hat{\boldsymbol{x}} - \boldsymbol{x}_d$ denotes an

estimation position error, $\boldsymbol{x}_d$ is the desired trajectory for the trapped cell, and $\dot{\boldsymbol{x}}_d$ is the desired velocity.

Multiplying both sides of equation (7) with $\boldsymbol{B}$ and substituting $-\boldsymbol{K}(\boldsymbol{x}-\boldsymbol{p})$ from equation (3), the observer dynamic equation is obtained as:

$$\boldsymbol{B}\dot{\boldsymbol{e}}_x + \boldsymbol{K}_x\boldsymbol{e}_x = \boldsymbol{0}, \tag{9}$$

which implies the convergence of $\boldsymbol{e}_x \rightarrow \boldsymbol{0}$. That is, the estimated position of cell converges to the actual position, $\hat{\boldsymbol{x}} \rightarrow \boldsymbol{x}$.

The observer based vision control method described by equations (7) and (8) is able to manipulate the trapped cell to track the desired trajectory without the measurement of the velocity of the cell. However, the exact knowledge of the damping matrix $\boldsymbol{B}$ is required for the desired position input $\boldsymbol{p}_d$, and hence parameter identification is necessary. In the case that the exact knowledge of the damping matrix is not available, an adaptive observer can be introduced to estimate the velocity of cell as:

$$\dot{\hat{\boldsymbol{x}}} = \hat{\boldsymbol{B}}^{-1}[-\boldsymbol{K}(\boldsymbol{x}-\boldsymbol{p}) + \boldsymbol{K}_x\boldsymbol{e}_x], \tag{10}$$

where $\hat{\boldsymbol{B}}$ is the estimated model for $\boldsymbol{B}$, and it is updated by the following update law:

$$\hat{\boldsymbol{\theta}}_s = \hat{\boldsymbol{\theta}}_s(0) - \boldsymbol{L}_s \int_0^t \boldsymbol{Y}_b^T(\dot{\hat{\boldsymbol{x}}})\boldsymbol{e}_x \mathrm{d}\varsigma. \tag{11}$$

In equation (11), $\hat{\boldsymbol{\theta}}_s$ is the vector of estimated parameters, $\hat{\boldsymbol{\theta}}_s(0)$ is any initial estimate of $\hat{\boldsymbol{\theta}}_s$, $\boldsymbol{L}_s$ is a positive definite matrix, and $\boldsymbol{Y}_b(\dot{\hat{\boldsymbol{x}}})$ is a dynamic regressor matrix [22], [39], while the term $\hat{\boldsymbol{B}}\dot{\hat{\boldsymbol{x}}}$ can be expressed in terms of the regressor as: $\hat{\boldsymbol{B}}\dot{\hat{\boldsymbol{x}}} = \boldsymbol{Y}_b(\dot{\hat{\boldsymbol{x}}})\hat{\boldsymbol{\theta}}_s$.

Next, a corresponding desired position input is proposed as:

$$\boldsymbol{p}_d = \hat{\boldsymbol{x}} - \boldsymbol{K}^{-1}\boldsymbol{K}_p\Delta\hat{\boldsymbol{x}} + \boldsymbol{K}^{-1}\boldsymbol{Y}_b(\dot{\boldsymbol{x}}_d)\hat{\boldsymbol{\theta}}_b. \tag{12}$$

and the uncertain parameters $\hat{\boldsymbol{\theta}}_b$ are updated by:

$$\hat{\boldsymbol{\theta}}_b = \hat{\boldsymbol{\theta}}_b(0) - \boldsymbol{L}_b \int_0^t \boldsymbol{Y}_b^T(\dot{\boldsymbol{x}}_d)\Delta\boldsymbol{x} \mathrm{d}\varsigma, \tag{13}$$

where $\Delta\boldsymbol{x} = \boldsymbol{x} - \boldsymbol{x}_d$ is the actual position error of the trapped cell, $\hat{\boldsymbol{\theta}}_b(0)$ is any initial estimate of $\hat{\boldsymbol{\theta}}_b$, $\boldsymbol{L}_b$ is a positive definite matrix, and $\boldsymbol{Y}_b(\dot{\boldsymbol{x}}_d)$ is also a regressor matrix. Similarly, we have: $\hat{\boldsymbol{B}}\dot{\boldsymbol{x}}_d = \boldsymbol{Y}_b(\dot{\boldsymbol{x}}_d)\hat{\boldsymbol{\theta}}_b$. The estimated position of the cell is used in equations (10) and (12), while the actual position of the cell $\boldsymbol{x}$ is employed to update the estimated parameters in equations (11) and (13).

Both the desired position input with the model-based observer (8) and the desired position input with the adaptive observer (12) are able to guarantee the convergence of tracking error and observation error, if $\Delta\boldsymbol{p} = \boldsymbol{0}$ and the control parameters $\boldsymbol{K}_p$ and $\boldsymbol{K}_x$ are chosen such that $\lambda_{min}[\boldsymbol{K}_p\boldsymbol{K}_x] > \frac{1}{4}\lambda_{max}[(\boldsymbol{K}-\boldsymbol{K}_p)^2]$, where $\lambda_{min}[\bullet]$ and $\lambda_{max}[\bullet]$ represent the minimum and the maximum eigenvalues respectively. The stability analysis for the controller with adaptive observer is given in the Appendix.

Remark 1: The simplified cell dynamics in equation (3) can be rewritten in state space as:

$$\dot{\boldsymbol{x}} = \boldsymbol{A}_x\boldsymbol{x} + \boldsymbol{B}_x\boldsymbol{p}, \tag{14}$$

where $\boldsymbol{A}_x = -\boldsymbol{B}^{-1}\boldsymbol{K}$, $\boldsymbol{B}_x = \boldsymbol{B}^{-1}\boldsymbol{K}$, and $\boldsymbol{y} = \boldsymbol{x}$ is the output. A Luenberger observer [40], [41] can also be developed based on the state-space model as:

$$\dot{\hat{\boldsymbol{x}}} = -\boldsymbol{B}^{-1}\boldsymbol{K}\hat{\boldsymbol{x}} + \boldsymbol{B}^{-1}\boldsymbol{K}\boldsymbol{p} + \boldsymbol{B}^{-1}\boldsymbol{K}_x\boldsymbol{e}_x. \tag{15}$$

Substituting equation (3) into the equation of Luenberger observer, we have: $\boldsymbol{B}\dot{\boldsymbol{e}}_x + (\boldsymbol{K}+\boldsymbol{K}_x)\boldsymbol{e}_x = \boldsymbol{0}$, which indicates the convergence of $\hat{\boldsymbol{x}} \rightarrow \boldsymbol{x}$. Since both the position of cell $\boldsymbol{x}$ and the position of laser $\boldsymbol{p}$ are measurable, it is also possible to replace the estimated position of cell with the actual position as in equation (7). △△△

B. Optical Manipulation of Cell with High Reynolds' Number

Next, we consider the case where the mass of the cell cannot be ignored. Let $\boldsymbol{s}_x \triangleq \dot{\boldsymbol{x}} - \dot{\hat{\boldsymbol{x}}}_r$ denote a sliding variable [42], where $\dot{\hat{\boldsymbol{x}}}_r$ is a reference vector to be defined later, the general dynamic model of the cell in equation (2) can be expressed in terms of the sliding variable $\boldsymbol{s}_x$ as:

$$\boldsymbol{M}\dot{\boldsymbol{s}}_x + \boldsymbol{B}\boldsymbol{s}_x + \boldsymbol{K}(\boldsymbol{x}-\boldsymbol{p}) + \boldsymbol{M}\ddot{\hat{\boldsymbol{x}}}_r + \boldsymbol{B}\dot{\hat{\boldsymbol{x}}}_r = \boldsymbol{0}, \tag{16}$$

where $\dot{\hat{\boldsymbol{x}}}_r = \dot{\boldsymbol{x}}_d - \alpha_x\Delta\hat{\boldsymbol{x}}$.

Suppose that the desired position input for the laser beam is denoted as $\boldsymbol{p}_d$, then equation (16) is written as:

$$\boldsymbol{M}\dot{\boldsymbol{s}}_x + \boldsymbol{B}\boldsymbol{s}_x + \boldsymbol{K}\boldsymbol{x} + \boldsymbol{M}\ddot{\hat{\boldsymbol{x}}}_r + \boldsymbol{B}\dot{\hat{\boldsymbol{x}}}_r = \boldsymbol{K}\boldsymbol{p}_d + \boldsymbol{K}\Delta\boldsymbol{p}. \tag{17}$$

Based on the dynamic model described by equation (17), a model-based observer is first developed to estimate the velocity of the cell as:

$$\ddot{\hat{\boldsymbol{x}}} = \boldsymbol{M}^{-1}[-\boldsymbol{K}(\boldsymbol{x}-\boldsymbol{p}) + \boldsymbol{K}_x\boldsymbol{e}_x - \boldsymbol{B}\dot{\hat{\boldsymbol{x}}}]. \tag{18}$$

Using the estimated velocity $\dot{\hat{\boldsymbol{x}}}$ and the estimated position $\hat{\boldsymbol{x}}$, the desired position input is proposed as:

$$\begin{aligned}\boldsymbol{p}_d = \hat{\boldsymbol{x}} &- \boldsymbol{K}^{-1}\boldsymbol{K}_p\Delta\hat{\boldsymbol{x}} - \boldsymbol{K}^{-1}\boldsymbol{K}_d(\Delta\dot{\hat{\boldsymbol{x}}} + \alpha_x\Delta\hat{\boldsymbol{x}}) \\ &+ \boldsymbol{K}^{-1}(\boldsymbol{M}\ddot{\hat{\boldsymbol{x}}}_r + \boldsymbol{B}\dot{\hat{\boldsymbol{x}}}_r),\end{aligned} \tag{19}$$

where $\Delta\dot{\hat{\boldsymbol{x}}} = \dot{\hat{\boldsymbol{x}}} - \dot{\boldsymbol{x}}_d$, $\boldsymbol{K}_p$ denotes the proportional control gain matrix which is diagonal and positive definite, and $\boldsymbol{K}_d$ denotes the control gain matrix of the sliding variable which is also diagonal and positive definite. Note that the actual velocity of the cell is also not required for the control method in equations (18) and (19).

Substituting equation (19) into equation (17), we have:

$$\boldsymbol{M}\dot{\boldsymbol{s}}_x + \boldsymbol{B}\boldsymbol{s}_x + \boldsymbol{K}\boldsymbol{e}_x + \boldsymbol{K}_p\Delta\hat{\boldsymbol{x}} + \boldsymbol{K}_d(\boldsymbol{s}_x - \dot{\boldsymbol{e}}_x) = \boldsymbol{K}\Delta\boldsymbol{p}. \tag{20}$$

Next, multiplying both sides of equation (18) with $\hat{\boldsymbol{M}}$ and substituting $-\boldsymbol{K}(\boldsymbol{x}-\boldsymbol{p})$ from equation (2), the observer dynamics is obtained as:

$$\boldsymbol{M}\ddot{\boldsymbol{e}}_x + \boldsymbol{B}\dot{\boldsymbol{e}}_x + \boldsymbol{K}_x\boldsymbol{e}_x = \boldsymbol{0}. \tag{21}$$

In the following theorem, we first consider the case when $\Delta\boldsymbol{p} = \boldsymbol{0}$ to show the convergence of the tracking errors. A control input of the manipulator of the laser source will be presented later to ensure the convergence of $\Delta\boldsymbol{p} \rightarrow \boldsymbol{0}$.

Theorem 1: *The desired position input of the laser beam in equation (19) and the observer in equation (18) for the optical manipulation system guarantee the convergence of* $\boldsymbol{x} \rightarrow \boldsymbol{x}_d$ *and*

$\dot{\boldsymbol{x}} \to \dot{\boldsymbol{x}}_d$ as $t \to \infty$ if $\Delta \boldsymbol{p} = \boldsymbol{0}$, and control gains $\boldsymbol{K}_p$, $\boldsymbol{K}_d$, α_x, and $\boldsymbol{K}_x$ are chosen to satisfy the following conditions:

$$\begin{gathered}\alpha_x \lambda_{min}[\boldsymbol{B} - \beta_x \boldsymbol{M}] > \tfrac{3}{4}\lambda_{max}[\boldsymbol{K}_p], \\ \lambda_{min}[(\boldsymbol{B}+\boldsymbol{K}_d)(\boldsymbol{B}-\beta_x \boldsymbol{M})] > \tfrac{3}{4}\lambda_{max}[\boldsymbol{K}_d^2], \\ \beta_x \lambda_{min}[\boldsymbol{K}_d \boldsymbol{K}_x] > \tfrac{1}{4}\lambda_{max}[\boldsymbol{K}^2], \\ \beta_x \lambda_{min}[\boldsymbol{K}_x(\boldsymbol{B}+\boldsymbol{K}_d)] > \tfrac{3}{4}\lambda_{max}[\boldsymbol{K}^2], \end{gathered} \tag{22}$$

where β_x is a positive constant such that $\beta_x < \lambda_{min}[\boldsymbol{B}\boldsymbol{M}^{-1}]$. In addition, the estimated position of the cell converges to the actual position such that $\hat{\boldsymbol{x}} \to \boldsymbol{x}$ as $t \to \infty$.

Proof: See Appendix. △△△

Remark 2: In the presence of uncertain cell dynamics, an adaptive observer is proposed to estimate the cell velocity as:

$$\ddot{\hat{\boldsymbol{x}}} = \hat{\boldsymbol{M}}^{-1}[-\boldsymbol{K}(\boldsymbol{x} - \boldsymbol{p}) + \boldsymbol{K}_x \boldsymbol{e}_x - \hat{\boldsymbol{B}}\dot{\hat{\boldsymbol{x}}}]. \tag{23}$$

The estimated models $\hat{\boldsymbol{M}}$ and $\hat{\boldsymbol{B}}$ are updated by the following update law as:

$$\begin{aligned}\hat{\boldsymbol{\theta}}_c = \hat{\boldsymbol{\theta}}_c(0) &- \boldsymbol{L}_c \boldsymbol{Y}_d^T(\dot{\hat{\boldsymbol{x}}}, \ddot{\hat{\boldsymbol{x}}})(\boldsymbol{e}_x + \beta_x \boldsymbol{\varepsilon}_x) \\ &+ \boldsymbol{L}_c \textstyle\int_0^t \dot{\boldsymbol{Y}}_d^T(\dot{\hat{\boldsymbol{x}}}, \ddot{\hat{\boldsymbol{x}}})(\boldsymbol{e}_x + \beta_x \boldsymbol{\varepsilon}_x) \mathrm{d}\varsigma, \end{aligned} \tag{24}$$

where $\boldsymbol{\varepsilon}_x = \int_0^t \boldsymbol{e}_x \mathrm{d}\varsigma$, $\hat{\boldsymbol{\theta}}_c$ is the vector of estimated parameters, $\hat{\boldsymbol{\theta}}_c(0)$ is any initial estimate of $\hat{\boldsymbol{\theta}}_c$, $\boldsymbol{L}_c$ is a positive definite matrix, $\boldsymbol{Y}_d(\dot{\hat{\boldsymbol{x}}}, \ddot{\hat{\boldsymbol{x}}})$ is a regressor matrix and $\hat{\boldsymbol{M}}\ddot{\hat{\boldsymbol{x}}} + \hat{\boldsymbol{B}}\dot{\hat{\boldsymbol{x}}} = \boldsymbol{Y}_d(\dot{\hat{\boldsymbol{x}}}, \ddot{\hat{\boldsymbol{x}}})\hat{\boldsymbol{\theta}}_c$. As seen from equation (24), only the actual position of the cell $\boldsymbol{x}$ is required to update the uncertain dynamic parameters $\hat{\boldsymbol{\theta}}_c$. In addition, the matrix $\dot{\boldsymbol{Y}}_d(\dot{\hat{\boldsymbol{x}}}, \ddot{\hat{\boldsymbol{x}}})$ represents the derivative of $\boldsymbol{Y}_d(\dot{\hat{\boldsymbol{x}}}, \ddot{\hat{\boldsymbol{x}}})$ which consists of the signal $\dddot{\hat{\boldsymbol{x}}}$. The signal $\dddot{\hat{\boldsymbol{x}}}$ is derived from the numerical differentiation of $\ddot{\hat{\boldsymbol{x}}}$, but it is then integrated again in the last term of the update law in equation (24).

Using the estimated velocity $\dot{\hat{\boldsymbol{x}}}$ and the estimated position $\hat{\boldsymbol{x}}$, a desired position input is proposed as:

$$\begin{aligned}\boldsymbol{p}_d = \hat{\boldsymbol{x}} &- \boldsymbol{K}^{-1}\boldsymbol{K}_p \Delta\hat{\boldsymbol{x}} - \boldsymbol{K}^{-1}\boldsymbol{K}_d(\Delta\dot{\hat{\boldsymbol{x}}} + \alpha_x \Delta\hat{\boldsymbol{x}}) \\ &+ \boldsymbol{K}^{-1}\boldsymbol{Y}_d(\dot{\hat{\boldsymbol{x}}}_r, \ddot{\hat{\boldsymbol{x}}}_r)\hat{\boldsymbol{\theta}}_d, \end{aligned} \tag{25}$$

where $\boldsymbol{Y}_d(\dot{\hat{\boldsymbol{x}}}_r, \ddot{\hat{\boldsymbol{x}}}_r)$ is also a regressor matrix, and $\hat{\boldsymbol{M}}\ddot{\hat{\boldsymbol{x}}}_r + \hat{\boldsymbol{B}}\dot{\hat{\boldsymbol{x}}}_r = \boldsymbol{Y}_d(\dot{\hat{\boldsymbol{x}}}_r, \dot{\hat{\boldsymbol{x}}}_r)\hat{\boldsymbol{\theta}}_d$. The uncertain dynamic parameters $\hat{\boldsymbol{\theta}}_d$ are updated as:

$$\begin{aligned}\hat{\boldsymbol{\theta}}_d = \hat{\boldsymbol{\theta}}_d(0) &- \boldsymbol{L}_d \boldsymbol{Y}_d^T(\dot{\hat{\boldsymbol{x}}}_r, \ddot{\hat{\boldsymbol{x}}}_r)(\boldsymbol{x} - \hat{\boldsymbol{x}}_r) \\ &+ \boldsymbol{L}_d \textstyle\int_0^t \dot{\boldsymbol{Y}}_d^T(\dot{\hat{\boldsymbol{x}}}_r, \ddot{\hat{\boldsymbol{x}}}_r)(\boldsymbol{x} - \hat{\boldsymbol{x}}_r) \mathrm{d}\varsigma, \end{aligned} \tag{26}$$

where $\boldsymbol{L}_d$ is a positive definite matrix, and $\hat{\boldsymbol{\theta}}_d(0)$ is any initial estimate of $\hat{\boldsymbol{\theta}}_d$.

To analyze the stability of the optical manipulation system, a Lyapunov-like candidate is introduced as:

$$\begin{aligned}V_c = &\tfrac{1}{2}\boldsymbol{s}_x^T \boldsymbol{M} \boldsymbol{s}_x + \tfrac{1}{2}\Delta\hat{\boldsymbol{x}}^T \boldsymbol{K}_p \Delta\hat{\boldsymbol{x}} + \tfrac{1}{2}\boldsymbol{z}_x^T \boldsymbol{M} \boldsymbol{z}_x \\ &+ \tfrac{1}{2}\Delta\boldsymbol{\theta}_d^T \boldsymbol{L}_d^{-1} \Delta\boldsymbol{\theta}_d + \tfrac{1}{2}\Delta\boldsymbol{\theta}_c^T \boldsymbol{L}_c^{-1} \Delta\boldsymbol{\theta}_c \\ &+ \tfrac{1}{2}\boldsymbol{e}_x^T[\boldsymbol{K}_x + \beta_x(\boldsymbol{B} - \beta_x \boldsymbol{M})]\boldsymbol{e}_x, \end{aligned} \tag{27}$$

where $\boldsymbol{z}_x = \dot{\boldsymbol{e}}_x + \beta_x \boldsymbol{e}_x$ is a sliding variable [42], $\Delta\boldsymbol{\theta}_d = \boldsymbol{\theta}_d - \hat{\boldsymbol{\theta}}_d$, and $\Delta\boldsymbol{\theta}_c = \boldsymbol{\theta}_c - \hat{\boldsymbol{\theta}}_c$. Differentiating V_c with respect to time, it can be shown that $\hat{\boldsymbol{x}} \to \boldsymbol{x}$, $\boldsymbol{x} \to \boldsymbol{x}_d$, $\dot{\boldsymbol{x}} \to \dot{\boldsymbol{x}}_d$ as $t \to \infty$. △△△

Remark 3: The positive constant α_x is the parameter for the sliding variable $\boldsymbol{s}_x$. The sliding variable $\boldsymbol{s}_x$ is a composite variable consisted of the position error $\Delta\hat{\boldsymbol{x}}$ and the velocity error $\Delta\dot{\boldsymbol{x}}$, and hence α_x can be treated as a weightage between these errors. Similarly, the positive constant β_x is the parameter for the sliding variable $\boldsymbol{z}_x$. The parameters α_x and β_x should be set to satisfy the conditions in equation (22) such that the stability of the system is guaranteed. △△△

C. Robotic Manipulation of Laser Source

The proposed desired position input $\boldsymbol{p}_d$ is able to manipulate the trapped cell to track the desired trajectory without measuring the velocity of the cell. In this section, we proceed to formulate a control input $\boldsymbol{u}$ for the manipulator of the laser beam, to guarantee that the actual position of the laser $\boldsymbol{p}$ tracks the desired position input $\boldsymbol{p}_d$ so that $\Delta\boldsymbol{p} \to \boldsymbol{0}$.

In the case that the camera is uncalibrated, the image Jacobian matrix is uncertain, and the estimated image-space velocity of laser beam is expressed as: $\dot{\hat{\boldsymbol{p}}} = \hat{\boldsymbol{J}}_I(\boldsymbol{q}, \hat{\boldsymbol{\theta}}_k)\dot{\boldsymbol{q}} = \boldsymbol{Y}_k(\boldsymbol{q}, \dot{\boldsymbol{q}})\hat{\boldsymbol{\theta}}_k$, where $\hat{\boldsymbol{J}}_I(\boldsymbol{q}, \hat{\boldsymbol{\theta}}_k)$ is the approximate image Jacobian matrix, $\hat{\boldsymbol{\theta}}_k$ is a set of estimated camera parameters, and $\boldsymbol{Y}_k(\boldsymbol{q}, \dot{\boldsymbol{q}})$ is a regressor matrix.

Using the estimated image Jacobian matrix, a sliding vector [42] is introduced as:

$$\boldsymbol{s}_q = \dot{\boldsymbol{q}} - \dot{\boldsymbol{q}}_r, \tag{28}$$

where $\dot{\boldsymbol{q}}_r = \hat{\boldsymbol{J}}_I^{-1}(\boldsymbol{q}, \hat{\boldsymbol{\theta}}_k)(\dot{\boldsymbol{p}}_d - \alpha_q \Delta\boldsymbol{p})$ is a reference vector, $\hat{\boldsymbol{J}}_I^{-1}(\boldsymbol{q}, \hat{\boldsymbol{\theta}}_k)$ is the inverse matrix of $\hat{\boldsymbol{J}}_I(\boldsymbol{q}, \hat{\boldsymbol{\theta}}_k)$, and α_q is a positive constant. Then the manipulator dynamic model in equation (4) can be expressed in terms of $\boldsymbol{s}_q$ as:

$$\boldsymbol{M}_q \dot{\boldsymbol{s}}_q + \boldsymbol{B}_q \boldsymbol{s}_q + \boldsymbol{Y}_q(\dot{\boldsymbol{q}}_r, \ddot{\boldsymbol{q}}_r)\boldsymbol{\theta}_q = \boldsymbol{u}, \tag{29}$$

where $\boldsymbol{\theta}_q$ is a vector of dynamic parameters, $\boldsymbol{Y}_q(\dot{\boldsymbol{q}}_r, \ddot{\boldsymbol{q}}_r)$ is a regressor matrix, and $\boldsymbol{M}_q \ddot{\boldsymbol{q}}_r + \boldsymbol{B}_q \dot{\boldsymbol{q}}_r = \boldsymbol{Y}_q(\dot{\boldsymbol{q}}_r, \ddot{\boldsymbol{q}}_r)\boldsymbol{\theta}_q$.

Next, the control input for the robotic manipulator of laser beam is proposed as:

$$\boldsymbol{u} = -\boldsymbol{K}_s \boldsymbol{s}_q - \hat{\boldsymbol{J}}_I^T(\boldsymbol{q}, \hat{\boldsymbol{\theta}}_k)\boldsymbol{K}_q \Delta\boldsymbol{p} + \boldsymbol{Y}_q(\dot{\boldsymbol{q}}_r, \ddot{\boldsymbol{q}}_r)\hat{\boldsymbol{\theta}}_q, \tag{30}$$

where $\boldsymbol{K}_s$ and $\boldsymbol{K}_q$ are diagonal and positive definite matrices. The estimated parameters $\hat{\boldsymbol{\theta}}_q$ and $\hat{\boldsymbol{\theta}}_k$ are updated by the following update law:

$$\begin{aligned}\hat{\boldsymbol{\theta}}_q &= \hat{\boldsymbol{\theta}}_q(0) - \boldsymbol{L}_q \textstyle\int_0^t \boldsymbol{Y}_q^T(\dot{\boldsymbol{q}}_r, \ddot{\boldsymbol{q}}_r)\boldsymbol{s}_q \mathrm{d}\varsigma, \\ \hat{\boldsymbol{\theta}}_k &= \hat{\boldsymbol{\theta}}_k(0) + \boldsymbol{L}_k \textstyle\int_0^t \boldsymbol{Y}_k^T(\boldsymbol{q}, \dot{\boldsymbol{q}})\boldsymbol{K}_q \Delta\boldsymbol{p} \mathrm{d}\varsigma, \end{aligned} \tag{31}$$

where $\hat{\boldsymbol{\theta}}_q(0)$ is any initial estimate of $\hat{\boldsymbol{\theta}}_q$, $\hat{\boldsymbol{\theta}}_k(0)$ is any initial estimate of $\hat{\boldsymbol{\theta}}_k$, and $\boldsymbol{L}_q$, $\boldsymbol{L}_k$ are positive definite matrices.

Substituting the control input (30) into equation (29), the closed-loop equation is given as:

$$\begin{gathered}\boldsymbol{M}_q \dot{\boldsymbol{s}}_q + (\boldsymbol{B}_q + \boldsymbol{K}_s)\boldsymbol{s}_q + \\ \hat{\boldsymbol{J}}_I^T(\boldsymbol{q}, \hat{\boldsymbol{\theta}}_k)\boldsymbol{K}_q \Delta\boldsymbol{p} + \boldsymbol{Y}_q(\dot{\boldsymbol{q}}_r, \ddot{\boldsymbol{q}}_r)\Delta\boldsymbol{\theta}_q = \boldsymbol{0}, \end{gathered} \tag{32}$$

where $\Delta\boldsymbol{\theta}_q = \boldsymbol{\theta}_q - \hat{\boldsymbol{\theta}}_q$. In the following theorem, we only consider the case that the cell with a low Reynolds' number is manipulated by using the desired position input $\boldsymbol{p}_d$ in equation (8) and the observer in equation (7). The stability of the optical manipulation system with the control methods described in equations (12), (19), and (25) can be similarly shown.

Theorem 2: *The input of the robotic manipulator (30), and*

the update law (31) for the robotic tweezers system ensure the convergence of the tracking errors, that is, $\boldsymbol{x} \to \boldsymbol{x}_d$, $\dot{\boldsymbol{x}} \to \dot{\boldsymbol{x}}_d$ as $t \to \infty$, when the control parameters are chosen so that:

$$\lambda_{min}[\boldsymbol{K}_p\boldsymbol{K}_x] > \tfrac{1}{4}\lambda_{max}[(\boldsymbol{K}-\boldsymbol{K}_p)^2], \quad \alpha_q\lambda_{min}[\boldsymbol{K}_p\boldsymbol{K}_q\boldsymbol{K}_x] > \tfrac{\alpha_q}{4}\lambda_{max}[\boldsymbol{K}_q\boldsymbol{K}_p\boldsymbol{K}_p] + \tfrac{1}{4}\lambda_{max}[\boldsymbol{K}_x\boldsymbol{K}^2]. \tag{33}$$

In addition, the estimated position of the cell converges to the actual position such that $\hat{\boldsymbol{x}} \to \boldsymbol{x}$ as $t \to \infty$.

Proof: See Appendix. △△△

Remark 4: The Cartesian-space velocity of the laser beam $\dot{\boldsymbol{q}}$ in the control input (30) is usually measurable. In the case that $\dot{\boldsymbol{q}}$ is not measurable, an observer can be developed similarly to estimate the velocity of the laser beam as:

$$\dot{\hat{\boldsymbol{q}}} = \boldsymbol{M}_q^{-1}(\boldsymbol{u} + \boldsymbol{K}_z\boldsymbol{e}_q - \boldsymbol{B}_q\dot{\hat{\boldsymbol{q}}}). \tag{34}$$

where $\boldsymbol{K}_z$ is a positive definite matrix, $\boldsymbol{e}_q = \boldsymbol{q} - \hat{\boldsymbol{q}}$ is the estimation error, $\hat{\boldsymbol{q}}$ is the estimated position of the laser beam, and $\dot{\hat{\boldsymbol{q}}}$ is the estimated velocity. △△△

Remark 5: The control input of the manipulator $\boldsymbol{u}$ in equation (30) requires $\ddot{\boldsymbol{q}}_r$ and thus $\ddot{\boldsymbol{p}}_d$. When the adaptive desired position input $\boldsymbol{p}_d$ in equations (12) or (25) is employed in the control input $\boldsymbol{u}$, the velocity of the cell is included in $\ddot{\boldsymbol{p}}_d$ due to the second-order differentiation of uncertain dynamic parameters $\hat{\boldsymbol{\theta}}_b$ and $\hat{\boldsymbol{\theta}}_d$ from equations (13) and (26). To solve the problem, another observer is required to construct the estimated desired position input $\hat{\boldsymbol{p}}_d$ as [22], [23]:

$$\begin{cases} \dot{\hat{\boldsymbol{p}}}_d = \boldsymbol{J}_I^T(\boldsymbol{q})\boldsymbol{\eta} + \beta(\boldsymbol{p}_d - \hat{\boldsymbol{p}}_d) \\ \dot{\boldsymbol{\eta}} = \boldsymbol{M}_q^{-1}[\boldsymbol{u} - \boldsymbol{B}_q\boldsymbol{\eta} + \boldsymbol{J}_I^T(\boldsymbol{q})\boldsymbol{K}_e(\boldsymbol{p}_d - \hat{\boldsymbol{p}}_d)], \end{cases} \tag{35}$$

where $\boldsymbol{\eta}$ is an auxiliary vector, β is a positive constant, and $\boldsymbol{K}_e$ is a positive definite matrix. △△△

Remark 6: In the case that the image Jacobian matrix is constant, the overall optical tweezers system with the dynamic equations (3) and (4) can also be rewritten as the state-space model as:

$$\begin{bmatrix} \dot{\boldsymbol{x}} \\ \dot{\boldsymbol{p}} \\ \ddot{\boldsymbol{q}} \end{bmatrix} = \begin{bmatrix} -\boldsymbol{B}^{-1}\boldsymbol{K} & \boldsymbol{B}^{-1}\boldsymbol{K} & \boldsymbol{0} \\ \boldsymbol{0} & \boldsymbol{0} & \boldsymbol{J}_I \\ \boldsymbol{0} & \boldsymbol{0} & -\boldsymbol{M}_q^{-1}\boldsymbol{B}_q \end{bmatrix} \begin{bmatrix} \boldsymbol{x} \\ \boldsymbol{p} \\ \dot{\boldsymbol{q}} \end{bmatrix} + \begin{bmatrix} \boldsymbol{0} \\ \boldsymbol{0} \\ \boldsymbol{M}_q^{-1}\boldsymbol{u} \end{bmatrix}, \tag{36}$$

where

$$\boldsymbol{y} = \begin{bmatrix} \boldsymbol{I}_2 & \boldsymbol{0} & \boldsymbol{0} \\ \boldsymbol{0} & \boldsymbol{I}_2 & \boldsymbol{0} \end{bmatrix} \begin{bmatrix} \boldsymbol{x} \\ \boldsymbol{p} \\ \dot{\boldsymbol{q}} \end{bmatrix} \tag{37}$$

is the output, $\boldsymbol{I}_2 \in \Re^{2\times 2}$ is an identity matrix, and $\boldsymbol{J}_I$ is the constant Jacobian matrix. Therefore, the Luenberger observer can also be developed similarly as model based observer for the whole optical manipulation system. △△△

IV. Simulation

Simulation studies were carried out to verify the performance of the proposed control methods. The optical tweezers system is illustrated in Fig. 4. In Fig. 4, the cell is placed on a motorized stage and the laser beam is fixed downwards, and the offset between the laser and the cell is varied by moving the stage which thus acts as a robotic manipulator.

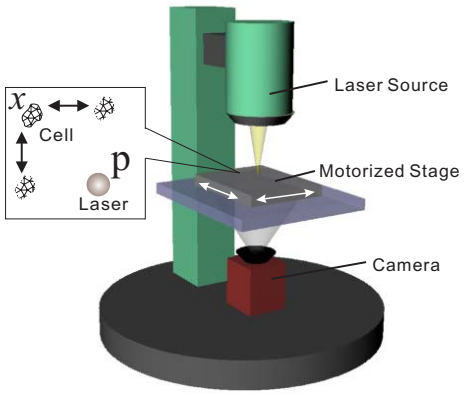

Fig. 4. The laser beam is fixed downwards, and the offset between the laser beam and the cell is varied by moving the stage with motor control.

In the simulation, we consider the case that the mass of the cell cannot be ignored such that the cell dynamics is specified in equation (2). Therefore, the interaction between the cell and the manipulator leads to an overall fourth-order dynamics described by equations (2) and (4). The parameters of the dynamic model in equation (2) were set as: the mass matrix $\boldsymbol{M}=diag\{10^{-10},10^{-10}\}kg$, the damping matrix $\boldsymbol{B}=diag\{1.8\times10^{-9},1.8\times10^{-9}\}kg/s$, and the trap stiffness matrix $\boldsymbol{K}=diag\{2.77\times10^{-5},2.77\times10^{-5}\}$. The parameters of the manipulator dynamics in equation (4) were set as: the mass matrix $\boldsymbol{M}_q = diag\{0.02218, 0.011386\}kg$, and the damping matrix $\boldsymbol{B}_q = diag\{0.04749, 0.04023\}kg/s$. The relationship between the Cartesian space and the image space is known as 0.1 μm/pixel, and the image Jacobian matrix is specified as: $\boldsymbol{J}_I = diag\{\beta_1,\beta_2\} = diag\{10,10\}$, where β_1 and β_2 are constants.

The initial positions of the cell and laser beam are both located at $(220, -150)$ pixel, and the cell was manipulated to follow the lemniscate of Bernoulli as:

$$\begin{cases} x_{d1} = 200 + \frac{20\cos(0.2t)}{1+\sin^2(0.2t)} \text{ pixel}, \\ x_{d2} = -150 + \frac{20\sin(0.2t)\cos(0.2t)}{1+\sin^2(0.2t)} \text{ pixel}. \end{cases} \tag{38}$$

Consider the dynamic model of the cell in equation (2), the observer in equation (18) and the desired position input $\boldsymbol{p}_d$ in equation (19) are employed for tracking control. The parameters of the observer are set as: $\boldsymbol{K}_x=30\boldsymbol{I}_2$. The observer is used to estimate the velocity and position of the cell.

The parameters of the desired position input in equation (19) were set as: $\alpha_x=32$, $\boldsymbol{K}_p=4\times10^{-8}\boldsymbol{I}_2$, and $\boldsymbol{K}_d=10^{-9}\boldsymbol{I}_2$. The desired position input $\boldsymbol{p}_d$ is able to manipulate the trapped cell to the desired trajectory without measuring the velocity of the cell.

In presence of the uncalibrated camera, the initial estimates of camera parameters are set as $\hat{\beta}_1(0)=\hat{\beta}_2(0)=9.5$. Therefore, the image Jacobian matrix is uncertain. The parameters of control methods in equations (30) and (31) were set as: $\alpha_q=1$, $\boldsymbol{K}_q = 1.5\boldsymbol{I}_2$, $\boldsymbol{K}_s = 10^{-5}\boldsymbol{I}_2$, $\boldsymbol{L}_k = 10^{-2}\boldsymbol{I}_2$, and $\boldsymbol{L}_q = 10^{-5}\boldsymbol{I}_4$ where $\boldsymbol{I}_4 \in \Re^{4\times4}$ is an identity matrix. The control input $\boldsymbol{u}$ ensures that the actual position of the laser $\boldsymbol{p}$ tracks the desired

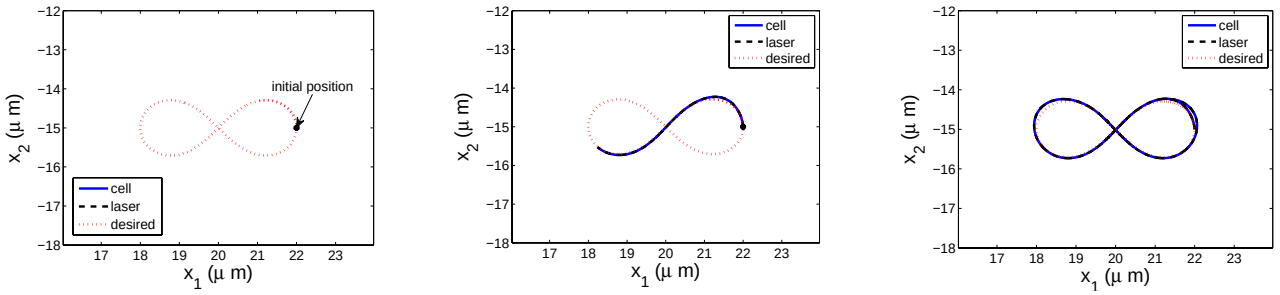

(a) t=0 s (b) t=15 s (c) t=35 s

Fig. 5. The cell is manipulated to track the desired Bernoulli trajectory which is specified as $x_{d1} = 200 + \frac{20\cos(0.2t)}{1+\sin^2(0.2t)}$ pixel, $x_{d2} = -150 + \frac{20\sin(0.2t)\cos(0.2t)}{1+\sin^2(0.2t)}$ pixel.

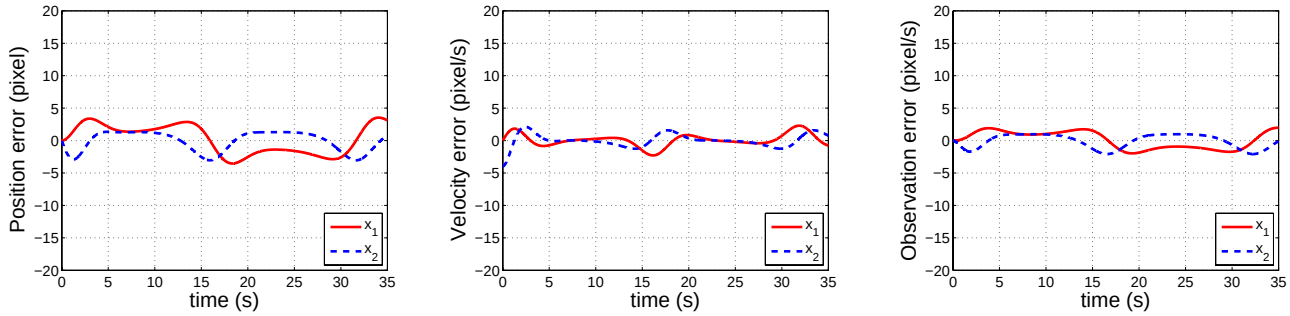

(a) position error $\boldsymbol{x} - \boldsymbol{x}_d$ (b) velocity error $\dot{\hat{\boldsymbol{x}}} - \dot{\boldsymbol{x}}_d$ (c) observation error $\dot{\boldsymbol{x}} - \dot{\hat{\boldsymbol{x}}}$

Fig. 6. Tracking errors and observation errors

position input $\boldsymbol{p}_d$ such that the convergence of tracking errors is guaranteed.

The path of the laser and the trapped cell at various time instants is shown in Fig. 5. From Fig. 5, it is seen that the cell was successfully manipulated to track the Bernoulli trajectory. The position error between the actual position of the cell and the desired position is denoted as $\boldsymbol{x} - \boldsymbol{x}_d$, which is less then 5 pixel as shown in Fig. 6(a). The velocity error between the estimated velocity of the cell and the desired velocity is denoted as $\dot{\hat{\boldsymbol{x}}} - \dot{\boldsymbol{x}}_d$, which is less than 5 pixel$/$s as shown in Fig. 6(b). The observation error is defined as $\dot{\boldsymbol{x}} - \dot{\hat{\boldsymbol{x}}}$, which is less than 3 pixel$/$s as shown in Fig. 6(c).

V. Experiment

The proposed control method was also implemented in a robotic tweezers manipulation system in the City University of Hong Kong, as shown in Fig. 7. The system is constituted of three modules for sensing, control and execution [19]. The sensing module consists of a microscope and a CCD camera, and the positions of biological cells and the laser beam can be obtained through image processing. The control module consists of a phase modulator and a stepping motor controller. The execution module consists of the holographic optical trapping and the motorized stage. All of the mechanical components are supported by an anti-vibration table.

The optical tweezers were controlled to manipulate the yeast cell. For the experimental environment, the Reynolds' number is around $3{\times}10^{-4}$ [19]. Therefore, the viscous drag dominates the inertia of the cell, and the cell dynamics is described by the simplified model in equation (3). Consider the simplified dynamic mode of the cell, the adaptive observer in equations (10) and (11) and the control method in equations (12) and (13) were implemented in the experimental setup.

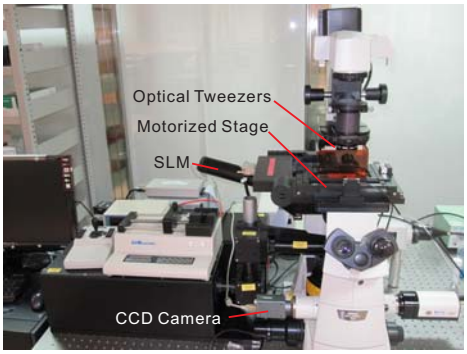

Fig. 7. A robot-tweezer manipulation system.

In the experiments, the position of the laser beam is fixed, and the relative position between the laser and the cell is varied by the motorized stage. Therefore, both the position of the cell and the position of the laser are specified with respect to the motorized stage. Due to the limited access to the software interface, the desired position $\boldsymbol{p}_d$ is set as the control input and implemented in the motorized stage. The relationship between the Cartesian space and the image space is known as 0.11 μm$/$pixel.

In the first experiment, both the cell and the laser beam started from $(17, 17)$ pixel, and the cell has been trapped by the laser beam from the beginning. The trapped cell was manipulated to track a straight line as:

$$\begin{cases} x_{d1} = 17 + 0.8t \text{ pixel}, \\ x_{d2} = 17 + 0.8t \text{ pixel}. \end{cases} \tag{39}$$

The control parameters in equations (10), (11), (12) and (13) were set as: $\boldsymbol{K}_p = \boldsymbol{I}_2$, $\boldsymbol{K}_x = \boldsymbol{I}_2$, $\boldsymbol{L}_b = 10^{-7}\boldsymbol{I}_2$, and $\boldsymbol{L}_s = 10^{-7}\boldsymbol{I}_2$. The regressor matrix $\boldsymbol{Y}_b(\dot{\boldsymbol{x}}_d)$ is specified as a diagonal matrix as: $\boldsymbol{Y}_b(\dot{\boldsymbol{x}}_d) = diag\{\dot{x}_{d1}, \dot{x}_{d2}\}$, and the vector $\hat{\boldsymbol{\theta}}_b = [\hat{b}_1, \hat{b}_2]^T$ where $\hat{b}_1$ and $\hat{b}_2$ represent the elements of the uncertain damping matrix $\hat{\boldsymbol{B}}$.

The path of the laser and the cell is shown in Fig. 8(a). Note that the positive direction in the axis of x_2 is downwards. Fig. 8(a) implies that the trapped cell is manipulated to track the straight line. The position error between the actual position of the cell and the desired position is denoted as $\boldsymbol{x} - \boldsymbol{x}_d$, while the velocity error between the estimated velocity of the cell and the desired velocity is denoted as $\dot{\hat{\boldsymbol{x}}} - \dot{\boldsymbol{x}}_d$. As seen from Fig. 8(b) and Fig. 8(c), and both the position error and the velocity error reduce to zero. The pictures of the trapped cell at different time instants are shown in Fig. 9, which implies the successful realization of tracking task without using the velocity of the cell.

In the second experiment, both the cell and the laser beam started from the initial position at $(43, 31)$ pixel, and the trapped cell was manipulated to track a circle as:

$$\begin{cases} x_{d1} = 33 + 10\cos(0.1t) \text{ pixel}, \\ x_{d2} = 31 + 10\sin(0.1t) \text{ pixel}. \end{cases} \tag{40}$$

The control parameters remain the same. The path of the laser and the cell is shown in Fig. 10(a), which shows that the position of the cell converges to the desired circular trajectory. The position error $\boldsymbol{x} - \boldsymbol{x}_d$ is shown in Fig. 10(b), which is less than 2 pixel throughout the manipulation. The velocity error $\dot{\hat{\boldsymbol{x}}} - \dot{\boldsymbol{x}}_d$ is shown in Fig. 10(c), which implies that the estimated velocity of the cell using the proposed observer converges to the desired velocity of the trapped cell. Next, the angular speed of the trajectory in equation (40) was increased from 0.1 rad/s to 0.2 rad/s, and the experimental results are shown in Fig. 11. As seen from Fig. 11, the proposed control method is still able to manipulate the trapped cell to track the circular trajectory, while the position error is less than 2 pixel and the velocity error is less than 1 pixel/s. The pictures of the trapped cell at different time instants for the angular speed 0.2 rad/s are shown in Fig. 12.

In the third experiment, both the cell and the laser beam started from $(58, 31)$ pixel, and the trapped cell was manipulated to track a Bernoulli trajectory as:

$$\begin{cases} x_{d1} = 48 + \frac{10\cos(0.1t)}{1+\sin^2(0.1t)} \text{ pixel}, \\ x_{d2} = 31 + \frac{10\sin(0.1t)\cos(0.1t)}{1+\sin^2(0.1t)} \text{ pixel}. \end{cases} \tag{41}$$

The control parameters remain the same. The path of the laser and the cell is shown in Fig. 13(a), which shows that the position of the cell converges to the desired Bernoulli trajectory. The position error $\boldsymbol{x} - \boldsymbol{x}_d$ is shown in Fig. 13(b), which is less than 1 pixel. The velocity error $\dot{\hat{\boldsymbol{x}}} - \dot{\boldsymbol{x}}_d$ is shown in Fig. 13(c), which reduces to zero. Next, the angular speed of the trajectory in equation (41) was increased from 0.1 rad/s to 0.2 rad/s, and the experimental results are shown in Fig. 14. As seen from Fig. 14, the proposed control method is still able to manipulate the trapped cell to track the Bernoulli trajectory, while the position error is less than 2 pixel and the velocity error is less than 1 pixel/s. The pictures of the trapped cell at different time instants for the angular speed 0.2 rad/s are shown in Fig. 15.

The experimental results indicate that all the trajectory and velocity tracking errors converge to small bounds at steady state, which shows the realization of the proposed methods.

VI. Conclusions

In this paper, vision-based observer techniques have been proposed for the optical manipulation with biological cells. Using the observer techniques, new tracking control methods are developed to manipulate the cell to track the desired trajectory without the information of the velocity of cell. The stability of closed-loop system is analyzed by using Lyapunov-like methods, and both simulations and experimental results are presented to illustrate the performance of the proposed methods. The proposed vision based observer techniques can be extended to other cell manipulation systems such as microinjection and micropipette. The proposed dynamic formulation would also bridge the gap between traditional robotic manipulation techniques and optical manipulation techniques. The development of the observer techniques are formulated in continuous time with the linear trapping force, and future work would be devoted to exploring the effects of limited sampling frequency and the time-varying trapping force, the uncertainties in the trapping stiffness on the system. The proposed observer techniques could also be extended to optical manipulation of multiple cells.

References

[1] S. J. Ralis, B. Vikramaditya, and B. J. Nelson, "Micropositioning of a weakly calibrated microassembly system using coarse-to-fine visual servoing strategies," *IEEE Trans. Electron. Pack.*, Vol. 23, No. 2, pp. 123-131, 2000.

[2] Y. Zhang, B. K. Chen, X. Liu, and Y. Sun, "Autonomous robotic pick-and-place of microobjects," *IEEE Trans. Robotics*, Vol. 26, No. 1, pp. 200-207, 2010.

[3] M. Rakotondrabe, and I. A. Ivan, "Development and force/position control of a new hybrid thermo-piezoelectric microgripper dedicated to micromanipulation tasks," *IEEE Trans. Autom. Sci. Eng.*, Vol. 8, No. 4, pp. 824-834, 2011.

[4] Y. Sun, and B. J. Nelson, "Biological cell injection using an autonomous microrobotic system," *Int. J. Robotics Res.*, Vol. 21, No. 10-11, pp. 861-868, 2002

[5] H. Huang, D. Sun, J. K. Mills, and S. H. Cheng, "Robotic cell injection system with position and force control: toward automatic batch biomanipulation," *IEEE Trans. Robotics*, Vol. 25, No. 3, pp. 727-737, 2009.

[6] X. Zhang, C, Leung, Z. Lu, N. Esfandiari, R. F. Casper, and Y. Sun, "Controlled aspiration and positioning of biological cells in a micropipette," *IEEE Trans. Biomed. Eng.*, Vol. 59, No. 4, pp. 1032-1040, 2012.

[7] E. Shojaei-Baghini, Y. Zheng, and Y. Sun, "Automated micropipette aspiration of single cells," *Ann. Biomed. Eng.*, Vol. 41, pp. 1208-1216, 2013.

[8] A. Ashkin, J. M. Dziedzic, J. E. Bjorkholm, and S. Chu, "Observation of a single beam gradient force optical trap for dielectric particles," *Opt. Letters*, Vol. 11, pp. 288-290, 1986.

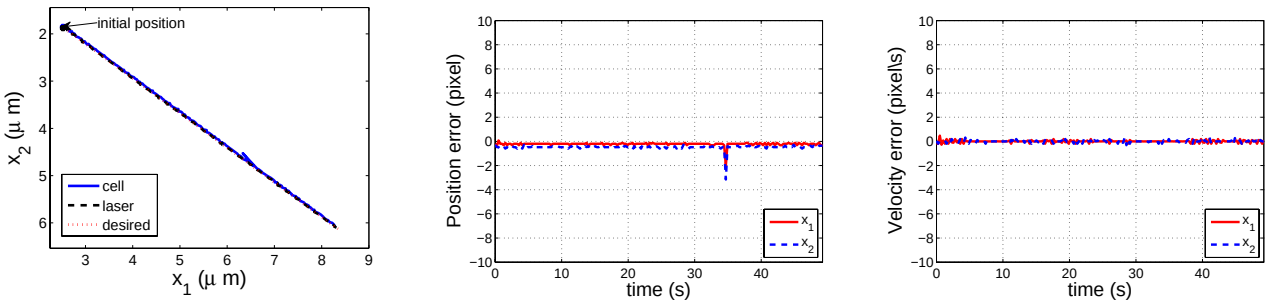

(a) path of the cell and the laser beam (b) position error $\boldsymbol{x} - \boldsymbol{x}_d$ (c) velocity error $\dot{\hat{\boldsymbol{x}}} - \dot{\boldsymbol{x}}_d$

Fig. 8. Experiment 1: Line tracking. The trapped cell started from $(17, 17)$ pixel and was manipulated to track a straight line as: $x_{d1} = 17 + 0.8t$ pixel, $x_{d2} = 17 + 0.8t$ pixel. Both the position error $\boldsymbol{x} - \boldsymbol{x}_d$ and the velocity error $\dot{\hat{\boldsymbol{x}}} - \dot{\boldsymbol{x}}_d$ reduce to zero.

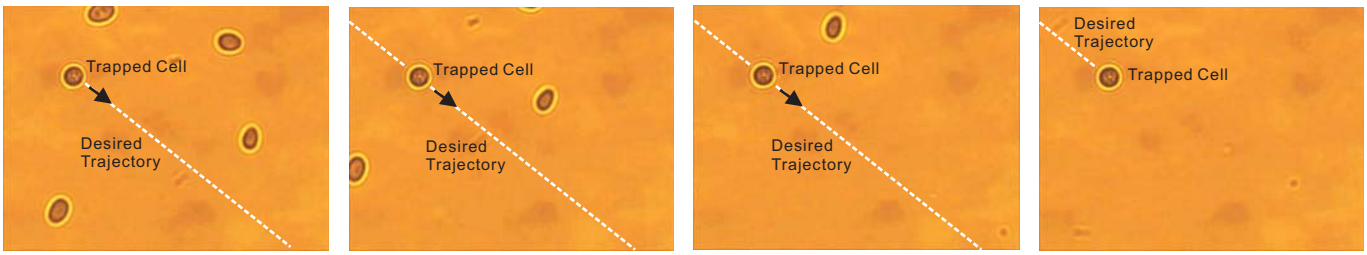

(a) t=0 s (b) t=10 s (c) t=20 s (d) t=30 s

Fig. 9. Experiment 1: The cell is manipulated to follow a straight line. The positions of the cell are shown at various time instants.

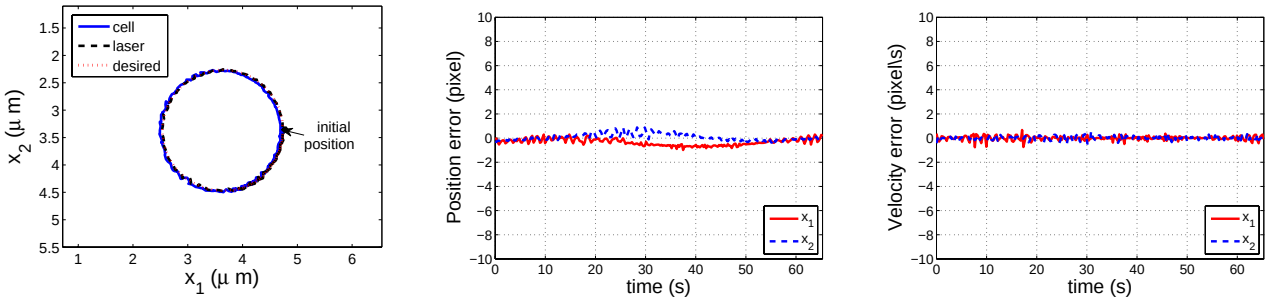

(a) path of the cell and the laser beam (b) position error $\boldsymbol{x} - \boldsymbol{x}_d$ (c) velocity error $\dot{\hat{\boldsymbol{x}}} - \dot{\boldsymbol{x}}_d$

Fig. 10. Experiment 2: Circle tracking. The trapped cell started from $(43, 31)$ pixel and was manipulated to track a circular trajectory as: $x_{d1} = 33 + 10\cos(0.1t)$ pixel, $x_{d2} = 31 + 10\sin(0.1t)$ pixel. The position error $\boldsymbol{x} - \boldsymbol{x}_d$ is less than 2 pixel and the velocity error $\dot{\hat{\boldsymbol{x}}} - \dot{\boldsymbol{x}}_d$ is less than 1 pixel/s.

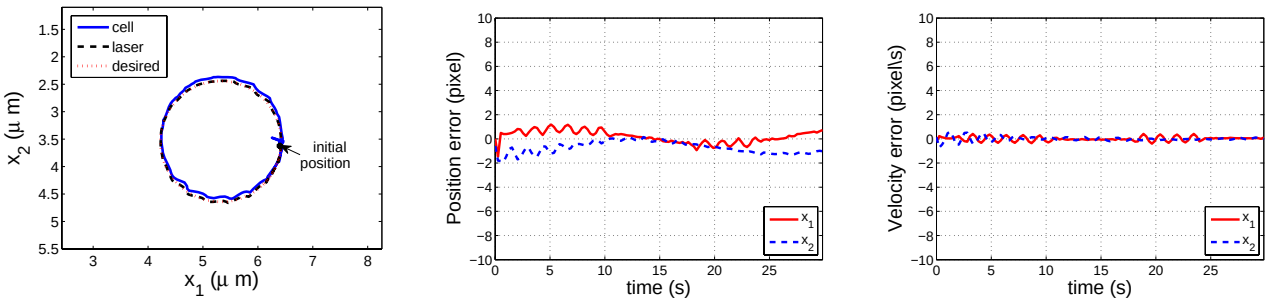

(a) path of the cell and the laser beam (b) position error $\boldsymbol{x} - \boldsymbol{x}_d$ (c) velocity error $\dot{\hat{\boldsymbol{x}}} - \dot{\boldsymbol{x}}_d$

Fig. 11. Experiment 2: Circle tracking. The angular velocity of the desired circular trajectory was increased to 0.2 rad/s.

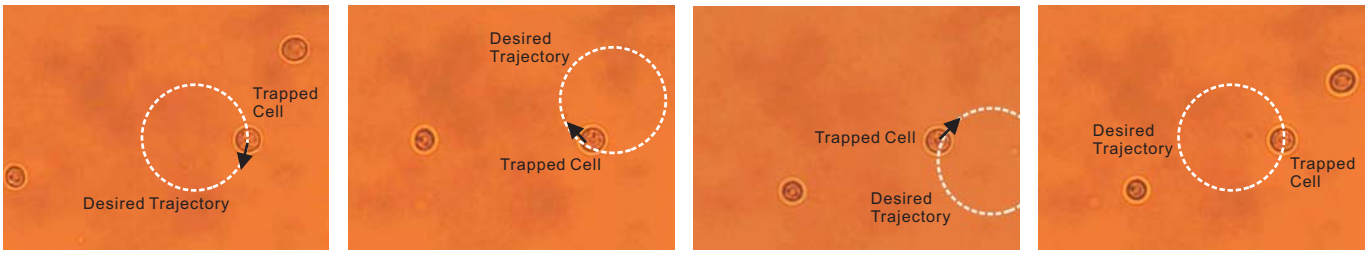

(a) t=0 s (b) t=10 s (c) t=20 s (d) t=30 s

Fig. 12. Experiment 2: The cell is manipulated to follow a circular trajectory with the angular velocity of 0.2 rad/s. The positions of the cell are shown at various time instants.

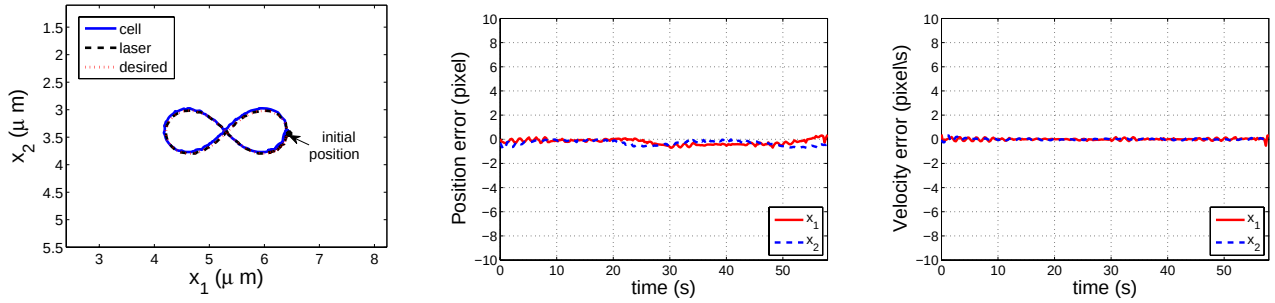

(a) path of the cell and the laser beam (b) position error $\boldsymbol{x} - \boldsymbol{x}_d$ (c) velocity error $\dot{\hat{\boldsymbol{x}}} - \dot{\boldsymbol{x}}_d$

Fig. 13. Experiment 3: Bernoulli tracking. The trapped cell started from $(58, 31)$ pixel and was manipulated to track a Bernoulli trajectory as: $x_{d1} = 48 + \frac{10\cos(0.1t)}{1+\sin^2(0.1t)}$ pixel, $x_{d2} = 31 + \frac{10\sin(0.1t)\cos(0.1t)}{1+\sin^2(0.1t)}$ pixel. The position error $\boldsymbol{x} - \boldsymbol{x}_d$ is less than 1 pixel and the velocity error $\dot{\hat{\boldsymbol{x}}} - \dot{\boldsymbol{x}}_d$ reduces to zero.

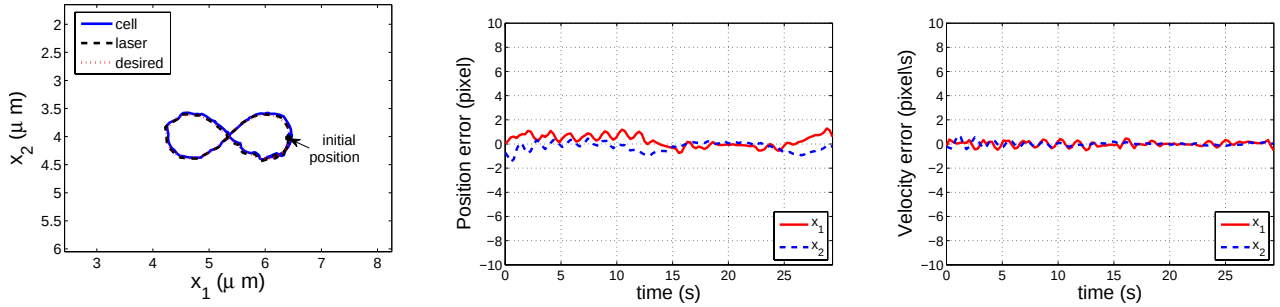

(a) path of the cell and the laser beam (b) position error $\boldsymbol{x} - \boldsymbol{x}_d$ (c) velocity error $\dot{\hat{\boldsymbol{x}}} - \dot{\boldsymbol{x}}_d$

Fig. 14. Experiment 3: Bernoulli tracking. The angular velocity of the desired Bernoulli trajectory was increased to 0.2 rad/s.

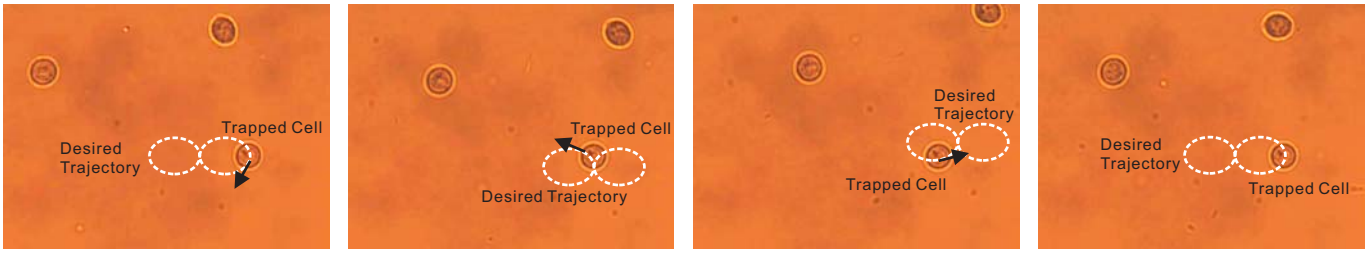

(a) t=0 s (b) t=10 s (c) t=20 s (d) t=30 s

Fig. 15. Experiment 3: The cell is manipulated to follow a Bernoulli trajectory with the angular velocity of 0.2 rad/s. The positions of the cell are shown at various time instants.

[9] A. Ashkin, "History of optical trapping and manipulation of small-neural particle, atoms, and molecules," *IEEE J. Sel. Top. Quant.*, Vol. 6, No. 6, pp. 841-856, 2000.

[10] S. C. Grover, A. G. Skirtach, R. C. Gauthier, and C. P. Grover, "Automated single-cell sorting system based on optical trapping," *J. Biomedical Optics*, Vol. 6, No. 1, pp. 14-22, 2001.

[11] Y. Tanaka, H. Kawada, K. Hirano, M. Ishikawa, and H. Kitajima, "Automated manipulation of non-spherical micro-objects using optical tweezers combined with image processing techniques," *Opt. Express*, Vol. 16, No. 19, pp. 15115-15122, 2008.

[12] Y. Huang, J. Wan, M. C. Cheng, Z. Zhang, S. Jhiang, and C. H. Menq, "Three-axis rapid steering of optically propelled micro/nanoparticles," *Rev. Sci. Instrum.*, Vol. 80, No. 6, 2009.

[13] A. Ranaweera, and B. Bamieh, "Modeling, identification and control of a spherical particle trapped in an optical tweezer," *Int. J. Robust Nonlin.*, Vol. 15, pp. 747-768, 2005.

[14] A. E. Wallin, H. Ojala, E. Haggstrom, and R. Tuma, "Stiffer optical tweezers through real-time feedback control," *Applied Physics Letters*, Vol. 92, 2008.

[15] J. Wan, Y. Huang, S. Jhiang, and C. H. Menq, "Real-time *in situ* calibration of an optically trapped probing system," *Appl. Opt.*, Vol. 48, No. 25, pp. 4832-4841, 2009.

[16] Y. Huang, Z. Zhang, and C. H. Menq, "Minimum-variance brownian motion control of an optically trapped probe," *Appl. Opt.*, Vol. 48, No. 3, pp. 5871-5880, 2009.

[17] Y. Huang, P. Cheng, and C. H. Menq, "Dynamic force sensing using an optically trapped probing system," *IEEE/ASME Trans. Mech.*, Vol. 16, No. 6, pp. 1145-1154, 2011.

[18] C. Aguilar-Ibanez, M. S. Suarez-Castanon, and L. I. Rosas-Soriano, "A simple control scheme for the manipulation of a particle by means of optical tweezers," *Int. J. Robust Nonlin.*, 2010.

[19] S. Hu, and D. Sun, "Automatic transportation of biological cells with a robot-tweezer manipulation system," *Int. J. Robotics Res.*, Vol. 30, No. 14, pp. 1681-1694, 2011.

[20] H. Chen, and D. Sun, "Moving groups of microparticles into array with a robot-tweezers manipulation system," *IEEE Trans. Robotics*, Vol. 28, No. 5, pp. 1069-1080, 2012.

[21] X. Li, and C. C. Cheah, "Dynamic region control for robot-assisted cell manipulation using optical tweezers," *IEEE Int. Conf. Robotics Automat.*, pp. 1057-1062, 2012.

[22] X. Li, C. C. Cheah, S. Hu, and D. Sun, "Dynamic trapping and manipulation of biological cells with optical tweezers," *Automatica*, Vol. 49, No. 6, pp. 1614-1625, 2013.

[23] X. Li, and C. C. Cheah, "Observer based adaptive control for optical manipulation of cell," *IEEE Int. Conf. Control, Automation, Robotics, Computer Vision*, pp. 1323-1328, 2012.

[24] S. Hutchinson, G. Hager, and P. Corke, "A tutorial on visual servo control," *IEEE Trans. Robotics Automat.*, Vol. 12, No. 5, pp. 651-670, 1996.

[25] C. C. Cheah, C. Liu, and J. J. E. Slotine, "Adaptive tracking controls for robots with unknown kinematics and dynamic properties," *Int. J. Robotics Res.*, Vol. 25, No. 3, pp. 283-296, 2006.

[26] S. Nicosia, and P. Tomei, "Robot control by using only joint position measurements," *IEEE Trans. Automatic Control*, Vol. 35, No. 9, pp. 1058-1061, 1990.

[27] H. Berghuis, and H. Nijmeijer, "A passivity approach to controller-observer design for robots," *IEEE Trans. Robotics Automat.*, Vol. 9, No. 6, pp. 740-754, 1993.

[28] M. Erlic, and W. S. Lu, "A reduced-order adaptive velocity observer for manipulator control," *EEE Trans. Robotics Automat.*, Vol. 11, No. 2, pp. 293-303, 1995.

[29] G. Bastin, and M. R. Gevers, "Stable adaptive observers for nonlinear time-varying systems," *IEEE Trans. Automatic Control*, Vol. 33, No. 7, pp. 650-658, 1988.

[30] Z. Hu, J. Zhang, and J. Liang, "Experimental measurement and analysis of the optical trapping force acting on a yeast cell with a lensed optical fiber probe," *Opt. Laser Tech.*, Vol. 39, No. 3, pp. 475-480, 2005.

[31] K. Svoboda, and S. M. Block, "Biological applications of optical forces," *Annu. Rev. Biophys. Biomol. Struct.*, Vol. 23, pp. 247-332, 1994.

[32] H. Oertel, "Prandtl's essentials of fluid mechanics," *Appl. Math. Sci.*, Vol. 158, pp. 118-125, 2004.

[33] F. Gittes, and C. H. Schmidt, "Signals and noise in micromechanical measurements," *Methods in Cell Biology*, Vol. 55, pp. 129-156, 1998.

[34] Y. H. Liu, H. Wang, C. Wang, and K. K. Lam, "Uncalibrated visual servoing of robots using a depth-independent interaction matrix," *IEEE Trans. Robotics*, Vol. 22, No. 4, pp. 804-817, 2006.

[35] B. Espiau, F. Chaumette, and P. Rives, "A new approach to visual servoing in robotics," *IEEE Trans. Robotics Automat.*, Vol. 8, No. 3, pp. 313-326, 1992.

[36] L. E. Weiss, A. C. Sanderson, and C. P. Neuman, "Dynamic sensor-based control of robots with visual feedback," *IEEE Trans. Robotics Automat.*, Vol. RA-3, No. 5, pp. 404-417, 1987.

[37] M. E. Justin, and P. J. Miles, "Lights, action: optical tweezers," *Contemporary Physics*, Vol. 43, No. 4, pp. 241-258, 2002.

[38] P. V. Kokotovic, "The joy of feedback: nonlinear and adaptive," *IEEE Control Systems Magazine*, Vol. 12, No. 3, pp. 7-17, 1992.

[39] J. J. E. Slotine, and W. Li, *Applied Nonlinear Control*. Englewood Cliffs, New Jersy: Prentice Hall, 1991.

[40] D. G. Luenberger, "Observers for multivariable systems", *IEEE Trans. Automatic Control*, Vol. 11, No. 2, pp. 190-197, 1966.

[41] D. G. Luenberger, "An introduction to observers", *IEEE Trans. Automatic Control*, Vol. 16, No. 6, pp. 596-602, 1971.

[42] J. J. E. Slotine, and W. Li, "On the adaptive control of robot manipulators," *Int J. Robotics Res.*, Vol. 6, No. 3, pp. 49-59, 1987.

[43] S. Arimoto, *Control Theory of Non-Linear Mechanical Systems*. Oxford University Press, 1996.

[44] M. W. Spong, and M. Vidyasagar, *Robot Dynamics and Control*. New York: John Wiley & Sons, 1989.

APPENDIX

A. Stability Analysis for Section III.A

Substituting the desired position input $\boldsymbol{p}_d$ in equation (12) into equation (6), we have:

$$\boldsymbol{B}\Delta\dot{\boldsymbol{x}}+(\boldsymbol{K}-\boldsymbol{K}_p)\boldsymbol{e}_x+\boldsymbol{K}_p\Delta\boldsymbol{x}+\boldsymbol{Y}_b(\dot{\boldsymbol{x}}_d)\Delta\boldsymbol{\theta}_b=\boldsymbol{K}\Delta\boldsymbol{p}, \quad (42)$$

where $\Delta\dot{\boldsymbol{x}}=\dot{\boldsymbol{x}}-\dot{\boldsymbol{x}}_d$, $\Delta\boldsymbol{\theta}_b=\boldsymbol{\theta}_b-\hat{\boldsymbol{\theta}}_b$ and $\boldsymbol{\theta}_b$ denote the actual dynamic parameters, and $(\boldsymbol{B}-\hat{\boldsymbol{B}})\dot{\boldsymbol{x}}_d=\boldsymbol{Y}_b(\dot{\boldsymbol{x}}_d)\Delta\boldsymbol{\theta}_b$. Next, multiplying equation (10) with $\hat{\boldsymbol{B}}$ and substituting $-\boldsymbol{K}(\boldsymbol{x}-\boldsymbol{p})$ in equation (3) into it, the dynamic equation of observer is obtained as:

$$\hat{\boldsymbol{B}}\dot{\hat{\boldsymbol{x}}}=\boldsymbol{B}\dot{\boldsymbol{x}}+\boldsymbol{K}_x\boldsymbol{e}_x. \quad (43)$$

The above equation can be written as:

$$\boldsymbol{B}\dot{\boldsymbol{e}}_x+\boldsymbol{K}_x\boldsymbol{e}_x+\boldsymbol{Y}_b(\dot{\hat{\boldsymbol{x}}})\Delta\boldsymbol{\theta}_s=\boldsymbol{0}, \quad (44)$$

where $\dot{\boldsymbol{e}}_x=\dot{\boldsymbol{x}}-\dot{\hat{\boldsymbol{x}}}$, $\Delta\boldsymbol{\theta}_s=\boldsymbol{\theta}_s-\hat{\boldsymbol{\theta}}_s$ and $\boldsymbol{\theta}_s$ denote the actual dynamic parameters, and $(\boldsymbol{B}-\hat{\boldsymbol{B}})\dot{\hat{\boldsymbol{x}}}=\boldsymbol{Y}_b(\dot{\hat{\boldsymbol{x}}})\Delta\boldsymbol{\theta}_s$.

To analyze the stability of the optical manipulation system with adaptive observer, a Lyapunov-like candidate is introduced as:

$$\begin{aligned}V_s=&\tfrac{1}{2}\Delta\boldsymbol{x}^T\boldsymbol{B}\Delta\boldsymbol{x}+\tfrac{1}{2}\boldsymbol{e}_x^T\boldsymbol{B}\boldsymbol{e}_x\\&+\tfrac{1}{2}\Delta\boldsymbol{\theta}_b^T\boldsymbol{L}_b^{-1}\Delta\boldsymbol{\theta}_b+\tfrac{1}{2}\Delta\boldsymbol{\theta}_s^T\boldsymbol{L}_s^{-1}\Delta\boldsymbol{\theta}_s,\end{aligned} \quad (45)$$

Differentiating V_s with respect to time, and substituting equations (42) and (44) into it yields:

$$\begin{aligned}\dot{V}_s=&\Delta\boldsymbol{x}^T\boldsymbol{B}\Delta\dot{\boldsymbol{x}}+\boldsymbol{e}_x^T\boldsymbol{B}\dot{\boldsymbol{e}}_x-\dot{\hat{\boldsymbol{\theta}}}_b^T\boldsymbol{L}_b^{-1}\Delta\boldsymbol{\theta}_b-\dot{\hat{\boldsymbol{\theta}}}_s^T\boldsymbol{L}_s^{-1}\Delta\boldsymbol{\theta}_s.\\=&\Delta\boldsymbol{x}^T[-(\boldsymbol{K}-\boldsymbol{K}_p)\boldsymbol{e}_x-\boldsymbol{K}_p\Delta\boldsymbol{x}-\boldsymbol{Y}_b(\dot{\boldsymbol{x}}_d)\Delta\boldsymbol{\theta}_b+\boldsymbol{K}\Delta\boldsymbol{p}]\\&+\boldsymbol{e}_x^T[-\boldsymbol{K}_x\boldsymbol{e}_x-\boldsymbol{Y}_b(\dot{\hat{\boldsymbol{x}}})\Delta\boldsymbol{\theta}_s]-\dot{\hat{\boldsymbol{\theta}}}_b^T\boldsymbol{L}_b^{-1}\Delta\boldsymbol{\theta}_b-\dot{\hat{\boldsymbol{\theta}}}_s^T\boldsymbol{L}_s^{-1}\Delta\boldsymbol{\theta}_s.\end{aligned} \quad (46)$$

Next, differentiating the update laws in equations (11) and (13) with respect to time and substituting them into equation (46), we have:

$$\dot{V}_s=\Delta\boldsymbol{x}^T\boldsymbol{K}\Delta\boldsymbol{p}-[\Delta\boldsymbol{x}^T\boldsymbol{e}_x^T]\boldsymbol{P}_s[\Delta\boldsymbol{x}^T\boldsymbol{e}_x^T]^T, \quad (47)$$

where

$$\boldsymbol{P}_s=\begin{bmatrix}\boldsymbol{K}_p & \frac{1}{2}\boldsymbol{K}-\frac{1}{2}\boldsymbol{K}_p\\ \frac{1}{2}\boldsymbol{K}-\frac{1}{2}\boldsymbol{K}_p & \boldsymbol{K}_x\end{bmatrix}. \quad (48)$$

If the control parameters $\boldsymbol{K}_p$ and $\boldsymbol{K}_x$ are chosen such that $\lambda_{min}[\boldsymbol{K}_p\boldsymbol{K}_x] > \frac{1}{4}\lambda_{max}[(\boldsymbol{K}-\boldsymbol{K}_p)^2]$, then $\boldsymbol{P}_s$ is positive definite. Then if $\Delta\boldsymbol{p}=\boldsymbol{0}$, we have that $V_s>0$, and $\dot{V}_s \leq 0$. Therefore, V_s is bounded, which also indicates that $\Delta\boldsymbol{x}$, $\boldsymbol{e}_x$, $\Delta\boldsymbol{\theta}_b$, and $\Delta\boldsymbol{\theta}_s$ are all bounded. From equation (42), it is concluded that $\Delta\dot{\boldsymbol{x}}$ is also bounded. The boundedness of $\Delta\dot{\boldsymbol{x}}$ ensures the boundedness of $\dot{\boldsymbol{x}}$ if $\dot{\boldsymbol{x}}_d$ is bounded. The boundedness of $\dot{\boldsymbol{x}}$ and $\boldsymbol{e}_x$ ensures the boundedness of $\dot{\hat{\boldsymbol{x}}}$ from equation (43). Since both $\dot{\boldsymbol{x}}$ and $\dot{\hat{\boldsymbol{x}}}$ are bounded, $\dot{\boldsymbol{e}}_x=\dot{\boldsymbol{x}}-\dot{\hat{\boldsymbol{x}}}$ is also bounded. Therefore, $\ddot{V}_s$ is bounded, and $\dot{V}_s$ is uniformly continuous. From the Barbalat's Lemma [39], we have $\dot{V}_s \to 0$ as $t\to\infty$. That is, $\boldsymbol{x}\to\boldsymbol{x}_d$ and $\boldsymbol{e}_x\to\boldsymbol{0}$.

In addition, the boundedness of $\Delta\boldsymbol{x}$ ensures the boundedness of $\dot{\hat{\boldsymbol{\theta}}}_b$ from equation (13). Differentiating equation (42), it is seen that $\Delta\ddot{\boldsymbol{x}}$ is bounded since $\Delta\dot{\boldsymbol{x}}$, $\dot{\hat{\boldsymbol{\theta}}}_b$, $\dot{\boldsymbol{e}}_x$ are bounded. Therefore, $\Delta\dot{\boldsymbol{x}}$ is uniformly continuous. Since $\Delta\boldsymbol{x}\to\boldsymbol{0}$ and $\Delta\dot{\boldsymbol{x}}$ is uniformly continuous, $\Delta\dot{\boldsymbol{x}}\to\boldsymbol{0}$. That is, $\dot{\boldsymbol{x}}\to\dot{\boldsymbol{x}}_d$.

Similarly, to analyze the stability of the optical manipulation system with the model-based observer in equation (7), a Lyapunov-like candidate V_{ms} is introduced as:

$$V_{ms}=\tfrac{1}{2}\Delta\boldsymbol{x}^T\boldsymbol{B}\Delta\boldsymbol{x}+\tfrac{1}{2}\boldsymbol{e}_x^T\boldsymbol{B}\boldsymbol{e}_x. \tag{49}$$

Differentiating V_{ms} with respect to time and substituting the dynamic equations of cell and observer into it, it is shown that:

$$\dot{V}_{ms}=\Delta\boldsymbol{x}^T\boldsymbol{K}\Delta\boldsymbol{p}-[\Delta\boldsymbol{x}^T\boldsymbol{e}_x^T]\boldsymbol{P}_s[\Delta\boldsymbol{x}^T\boldsymbol{e}_x^T]^T. \tag{50}$$

Therefore, the convergence of tracking error and observation error is also guaranteed if $\Delta\boldsymbol{p}$=$\boldsymbol{0}$ and $\boldsymbol{P}_s$ is positive definite.

B. Proof of Theorem 1

To analyze the stability of the optical manipulation system, a Lyapunov-like candidate V_{mc} is introduced as:

$$\begin{aligned}V_{mc}=&\tfrac{1}{2}\boldsymbol{s}_x^T\boldsymbol{M}\boldsymbol{s}_x+\tfrac{1}{2}\Delta\hat{\boldsymbol{x}}^T\boldsymbol{K}_p\Delta\hat{\boldsymbol{x}}+\tfrac{1}{2}\boldsymbol{z}_x^T\boldsymbol{M}\boldsymbol{z}_x\\&+\tfrac{1}{2}\boldsymbol{e}_x^T[\boldsymbol{K}_x+\beta_x(\boldsymbol{B}-\beta_x\boldsymbol{M})]\boldsymbol{e}_x.\end{aligned} \tag{51}$$

Differentiating V_{mc} with respect to time and substituting equations (20), and (21) into it, we have:

$$\begin{aligned}\dot{V}_{mc}=&-\boldsymbol{s}_x^T(\boldsymbol{B}+\boldsymbol{K}_d)\boldsymbol{s}_x-\boldsymbol{s}_x^T\boldsymbol{K}\boldsymbol{e}_x+\boldsymbol{s}_x^T\boldsymbol{K}_d\dot{\boldsymbol{e}}_x-\boldsymbol{s}_x^T\boldsymbol{K}_p\Delta\hat{\boldsymbol{x}}\\&+\beta_x\boldsymbol{z}_x^T\boldsymbol{M}\dot{\boldsymbol{e}}_x-\boldsymbol{z}_x^T\boldsymbol{B}\dot{\boldsymbol{e}}_x-\boldsymbol{z}_x^T\boldsymbol{K}_x\boldsymbol{e}_x\\&+\boldsymbol{s}_x^T\boldsymbol{K}\Delta\boldsymbol{p}+\Delta\dot{\hat{\boldsymbol{x}}}^T\boldsymbol{K}_p\Delta\hat{\boldsymbol{x}}+\dot{\boldsymbol{e}}_x^T[\boldsymbol{K}_x+\beta_x(\boldsymbol{B}-\beta_x\boldsymbol{M})]\boldsymbol{e}_x.\end{aligned} \tag{52}$$

Note that $\boldsymbol{s}_x=\Delta\dot{\boldsymbol{x}}+\alpha_x\Delta\hat{\boldsymbol{x}}=\Delta\dot{\hat{\boldsymbol{x}}}+\dot{\boldsymbol{e}}_x+\alpha_x\Delta\hat{\boldsymbol{x}}$, and $\boldsymbol{z}_x=\dot{\boldsymbol{e}}_x+\beta_x\boldsymbol{e}_x$, and thus equation (52) can be written as:

$$\dot{V}_{mc}=-[\boldsymbol{s}_x^T\Delta\hat{\boldsymbol{x}}^T\boldsymbol{e}_x^T\dot{\boldsymbol{e}}_x^T]\boldsymbol{P}_c[\boldsymbol{s}_x^T\Delta\hat{\boldsymbol{x}}^T\boldsymbol{e}_x^T\dot{\boldsymbol{e}}_x^T]^T+\boldsymbol{s}_x^T\boldsymbol{K}\Delta\boldsymbol{p}, \tag{53}$$

where

$$\boldsymbol{P}_c=\begin{bmatrix}\boldsymbol{B}+\boldsymbol{K}_d & \boldsymbol{0} & \frac{1}{2}\boldsymbol{K} & -\frac{1}{2}\boldsymbol{K}_d\\ \boldsymbol{0} & \alpha_x\boldsymbol{K}_p & \boldsymbol{0} & \frac{1}{2}\boldsymbol{K}_p\\ \frac{1}{2}\boldsymbol{K} & \boldsymbol{0} & \beta_x\boldsymbol{K}_x & \boldsymbol{0}\\ -\frac{1}{2}\boldsymbol{K}_d & \frac{1}{2}\boldsymbol{K}_p & \boldsymbol{0} & \boldsymbol{B}-\beta_x\boldsymbol{M}\end{bmatrix}. \tag{54}$$

If the control parameters α_x, β_x, $\boldsymbol{K}_d$, $\boldsymbol{K}_p$, and $\boldsymbol{K}_x$ are chosen to satisfy condition (22), then $\boldsymbol{P}_c$ is positive definite.

Since $\Delta\boldsymbol{p}=\boldsymbol{0}$, we have that $V_{mc}>0$, and $\dot{V}_{mc}\leq 0$ if condition (22) is satisfied. Therefore, V_{mc} is bounded, which also indicates that $\boldsymbol{s}_x$, $\Delta\hat{\boldsymbol{x}}$, $\boldsymbol{e}_x$, and $\boldsymbol{z}_x$ are all bounded. The boundedness of $\boldsymbol{s}_x$ and $\Delta\hat{\boldsymbol{x}}$ ensures the boundedness of $\Delta\dot{\boldsymbol{x}}$ since $\boldsymbol{s}_x=\Delta\dot{\boldsymbol{x}}+\alpha_x\Delta\hat{\boldsymbol{x}}$, and the boundedness of $\boldsymbol{z}_x$ and $\boldsymbol{e}_x$ ensures the boundedness of $\dot{\boldsymbol{e}}_x$ since $\boldsymbol{z}_x=\dot{\boldsymbol{e}}_x+\beta_x\boldsymbol{e}_x$. Since both $\Delta\dot{\boldsymbol{x}}$ and $\dot{\boldsymbol{e}}_x$ are bounded, $\Delta\dot{\hat{\boldsymbol{x}}}=\Delta\dot{\boldsymbol{x}}-\dot{\boldsymbol{e}}_x$ is also bounded. From equation (20), since $\boldsymbol{s}_x$, $\boldsymbol{e}_x$, $\dot{\boldsymbol{e}}_x$, and $\Delta\hat{\boldsymbol{x}}$ are all bounded, $\dot{\boldsymbol{s}}_x$ is also bounded. Therefore, $\boldsymbol{s}_x$, $\Delta\hat{\boldsymbol{x}}$, and $\boldsymbol{e}_x$ are uniformly continuous. From equation (53), it is easy to verify that $\boldsymbol{s}_x, \Delta\hat{\boldsymbol{x}}, \boldsymbol{e}_x \in L_2(0,+\infty)$. Then it follows [43], [44] that $\boldsymbol{s}_x, \Delta\hat{\boldsymbol{x}}, \boldsymbol{e}_x \to \boldsymbol{0}$ and hence $\hat{\boldsymbol{x}}\to\boldsymbol{x}$. Since $\Delta\hat{\boldsymbol{x}}, \boldsymbol{e}_x\to\boldsymbol{0}$, we have $\boldsymbol{x}\to\boldsymbol{x}_d$ as $t\to\infty$. Since $\boldsymbol{s}_x\to\boldsymbol{0}$ and $\Delta\hat{\boldsymbol{x}}\to\boldsymbol{0}$, we have $\dot{\boldsymbol{x}}\to\dot{\boldsymbol{x}}_d$ as $t\to\infty$.

C. Proof of Theorem 2

Substituting the desired position input in equation (8) into the simplified cell dynamics in equation (6), we have:

$$\boldsymbol{B}\Delta\dot{\boldsymbol{x}}+(\boldsymbol{K}-\boldsymbol{K}_p)\boldsymbol{e}_x+\boldsymbol{K}_p\Delta\boldsymbol{x}=\boldsymbol{K}\Delta\boldsymbol{p}. \tag{55}$$

To prove the stability, a Lyapunov-like candidate V is introduced as:

$$\begin{aligned}V=&\tfrac{1}{2}\Delta\boldsymbol{x}^T\boldsymbol{B}\Delta\boldsymbol{x}+\tfrac{1}{2}\boldsymbol{e}_x^T\boldsymbol{B}\boldsymbol{e}_x+\tfrac{1}{2}\boldsymbol{s}_q^T\boldsymbol{M}_q\boldsymbol{s}_q\\&+\tfrac{1}{2}\Delta\boldsymbol{p}^T\boldsymbol{K}_q\Delta\boldsymbol{p}+\tfrac{1}{2}\Delta\boldsymbol{\theta}_q^T\boldsymbol{L}_q^{-1}\Delta\boldsymbol{\theta}_q+\tfrac{1}{2}\Delta\boldsymbol{\theta}_k^T\boldsymbol{L}_k^{-1}\Delta\boldsymbol{\theta}_k.\end{aligned} \tag{56}$$

Differentiating V with respect to time and substituting equations (55), (9), (32), and the update law (31) into it, we have:

$$\begin{aligned}\dot{V}=&\Delta\boldsymbol{x}^T(\boldsymbol{K}_p-\boldsymbol{K})\boldsymbol{e}_x-\Delta\boldsymbol{x}^T\boldsymbol{K}_p\Delta\boldsymbol{x}+\Delta\boldsymbol{x}^T\boldsymbol{K}\Delta\boldsymbol{p}\\&-\boldsymbol{s}_q^T(\boldsymbol{B}_q+\boldsymbol{K}_s)\boldsymbol{s}_q-\alpha_q\Delta\boldsymbol{p}^T\boldsymbol{K}_q\Delta\boldsymbol{p}-\boldsymbol{e}_x^T\boldsymbol{K}_x\boldsymbol{e}_x\\=&-\boldsymbol{s}_q^T(\boldsymbol{B}_q+\boldsymbol{K}_s)\boldsymbol{s}_q-[\Delta\boldsymbol{x}^T\boldsymbol{e}_x^T\Delta\boldsymbol{p}^T]\boldsymbol{P}[\Delta\boldsymbol{x}^T\boldsymbol{e}_x^T\Delta\boldsymbol{p}^T]^T,\end{aligned} \tag{57}$$

where

$$\boldsymbol{P}=\begin{bmatrix}\boldsymbol{K}_p & \frac{1}{2}\boldsymbol{K}-\frac{1}{2}\boldsymbol{K}_p & -\frac{1}{2}\boldsymbol{K}\\ \frac{1}{2}\boldsymbol{K}-\frac{1}{2}\boldsymbol{K}_p & \boldsymbol{K}_x & \boldsymbol{0}\\ -\frac{1}{2}\boldsymbol{K} & \boldsymbol{0} & \alpha_q\boldsymbol{K}_q\end{bmatrix}. \tag{58}$$

Let the controller parameters $\boldsymbol{K}_p$, α_q, $\boldsymbol{K}_q$ and $\boldsymbol{K}_x$ be chosen to satisfy the condition (33), then $\boldsymbol{P}$ is positive definite. In the case that $\boldsymbol{P}$ is positive definite, $\dot{V}\leq 0$.

Since $V>0$ and $\dot{V}\leq 0$, V is bounded. The boundedness of V ensures the boundedness of $\Delta\boldsymbol{x}$, $\boldsymbol{s}_q$, $\Delta\boldsymbol{p}$, $\boldsymbol{e}_x$, $\Delta\boldsymbol{\theta}_q$, and $\Delta\boldsymbol{\theta}_k$. From equations (55) and (9), it is concluded that $\dot{\boldsymbol{x}}$ and $\dot{\boldsymbol{e}}_x$ are bounded, and hence $\dot{\hat{\boldsymbol{x}}}=\dot{\boldsymbol{x}}-\dot{\boldsymbol{e}}_x$ is bounded. From equation (8), $\dot{\boldsymbol{p}}_d$ is also bounded because $\dot{\hat{\boldsymbol{x}}}$ is bounded. The boundedness of $\boldsymbol{s}_q$, $\Delta\boldsymbol{p}$ and $\dot{\boldsymbol{p}}_d$ ensures the boundedness of $\dot{\boldsymbol{q}}$, and the boundedness of $\dot{\boldsymbol{q}}$ ensures the boundedness of $\dot{\boldsymbol{p}}$ since $\boldsymbol{J}_I(\boldsymbol{q})$ is bounded. Since $\dot{\boldsymbol{p}}$ and $\dot{\boldsymbol{p}}_d$ are bounded, $\Delta\dot{\boldsymbol{p}}$ is bounded. Therefore, $\Delta\boldsymbol{p}$ is uniformly continuous. From equation (57), it is easy to verify that $\Delta\boldsymbol{p}\in L_2(0,+\infty)$. Then it follows [43], [44] that $\Delta\boldsymbol{p}\to\boldsymbol{0}$. Therefore, $\boldsymbol{x}\to\boldsymbol{x}_d$, $\dot{\boldsymbol{x}}\to\dot{\boldsymbol{x}}_d$, and $\hat{\boldsymbol{x}}\to\boldsymbol{x}$ as $t\to\infty$.

Chien Chern CHEAH was born in Singapore. He received B.Eng. degree in Electrical Engineering from National University of Singapore in 1990, M.Eng. and Ph.D. degrees in Electrical Engineering, both from Nanyang Technological University, Singapore, in 1993 and 1996, respectively.

From 1990 to 1991, he worked as a design engineer in Chartered Electronics Industries, Singapore. He was a research fellow in the Department of Robotics, Ritsumeikan University, Japan from 1996 to 1998. He joined the School of Electrical and Electronic Engineering, Nanyang Technological University as an assistant professor in 1998. Since 2003, he has been an associate professor in Nanyang Technological University. In November 2002, he received the oversea attachment fellowship from the Agency for Science, Technology and Research (A*STAR), Singapore to visit the Nonlinear Systems laboratory, Massachusetts Institute of Technology. He serves as an associate editor for IEEE Transactions on Robotics, Automatica and Asian Journal of Control.

Xiang LI received the Bachelor, Master and PhD degrees from Beijing Institute of Technology, and Nanyang Technological University in 2006, 2008, and 2013 respectively. He is currently working as a Research Fellow at the Intelligent Robotics Lab, Nanyang Technological University, Singapore.

Xiang LI has served as a reviewer for several international journals including Automatica, IEEE Transactions on Robotics, IEEE Transactions on Mechatronics, and Asian Journal of Control. He was awarded Highly Commended Paper Award in the 3rd IFToMM International Symposium on Robotics and Mechatronics. His current research interests include robot control, visual servoing, and cell manipulation.

Xiao Yan received the Bachelor and PhD degrees from City University of Hong Kong in 2009 and 2013 respectively. He is currently working as a Research Fellow at the Intelligent Robotics Lab, Nanyang Technological University, Singapore. His current research interests include multirobot control and cell manipulation.

Dong SUN (S'95-A'97-M'00-SM'08) is currently a chair professor in the Department of Mechanical and Biomedical Engineering, City University of Hong Kong. He received the Bachelor and Master's degrees in mechatronics and biomedical engineering from Tsinghua University, Beijing, China, and the Ph.D. degree in robotics and automation from the Chinese University of Hong Kong, Hong Kong. Before he joined City University of Hong Kong in 2000, he was a Postdoctoral researcher at the University of Toronto, Toronto, ON, Canada, and a Research and Development Engineer in Ontario industry. Prof. Sun has research interests in robot-aided cell manipulation, multirobot systems, and motion controls. He was an Associate Editor for the IEEE Transactions on Robotics from 2004 to 2008. He currently serves as a Technical Editor for the IEEE/ASME Transactions on Mechatronics.